Relationship Between Crude Oil Composition and Physical-Chemical Properties.

By Yvonne Kolltveit

Master Thesis

Department of Chemistry
Faculty of Mathematics and Natural Science
University of Bergen
June 2016

Abstract

Improving oil recovery by low salinity waterflooding has been of interest in both laboratories and fields in recent years. Understanding how the underlying mechanism affects the final recovery is necessary in order to optimize waterflooding and chemical injection.

A physical-chemical investigation of the crude oil/brine/reservoir rock system, and correlation with crude oil composition, is the focus of this thesis. Three crude oils from different fields in the North Sea have been investigated. Interactions between the crude oils and brine were investigated by studies of interfacial tension and zeta potentials. Contact angles were studied to examine the wettability behaviour in the crude oil/brine/rock system. The interactions were studied as a function of brine pH and ionic strength.

A decrease in interfacial tension and zeta potential with increasing pH and ionic strength, was observed for all crude oils. A presence of small amounts of divalent calcium cations were found to increase the interfacial tension at pH 11, but decrease the interfacial tension at pH 9. It proved difficult to identify any trends in the contact angle measurements, however one of the crude oils appeared to have higher contact angles than the others. The crude oil with lowest acidity, was found to have the highest interfacial activity. The lowest interfacial activity was observed for the crude oil with the highest asphaltene content.

Acknowledgements

First of all, I want to thank Kristine Spildo for her exceptional guidance throughout this work. Her ability to impart knowledge, her patience and constructive feedback has been highly appreciated. I would also like to thank Tanja Barth for her guidance and for always being available to answer my questions. Also, thank you to Tore Skodvin for all your help.

I also want to thank my fellow students in "the office". Thank you for making every day a fun day. A special thanks to Gine, for her excellent support and cooperation during this thesis. Further, thanks to friends and family for the support and patience they have provided.

Thank you,

Yvonne Kolltveit

Abbreviations and Symbols

Abbreviations

API	American Petroleum Institute
COB	Crude Oil/Brine
COBR	Crude Oil/Brine/Rock
DLVO	Deryaguin, Landau, Verwey, Overbeek
EDL	Electrical Double Layer
e.g.	For Example
EOR	Enhanced Oil Recovery
et al.	And Others
IEP	Isoelectric Point
IFT	Interfacial Tension
IOR	Improved Oil Recovery
NSO	Nitrogen, Sulphur, Oxygen
OCA	Optical Contact Angle
SP	Specific Gravity
TAN	Total Acid Number
TBN	Total Base Number

Symbols

κ^{-1}	Debye Length [nm]
ζ	Zeta Potential [mV]
θ	Contact Angle [°]
γ	Interfacial Tension [mN/m]
ΔP	Capillary Pressure
I	Ionic Strength [$mol \cdot L^{-1}$]
pK_a	Acid Dissociation Constant [a.u.]
z	Ion Valance [a.u.]
ρ	Density [$g \cdot cm^{-3}$]

m	Mass [g]
F	Relative Humidity [%]
wt%	Weight Percent [g/100g]
C	Molar Concentration [$mol \cdot L^{-1}$]
X_{Ca}	Mole Fraction of Calcium [a.u.]
g	Acceleration of Gravity [$m \cdot s^{-2}$]
σ	Standard Deviation [a.u.]
ν	Velocity [$m \cdot s^{-2}$]
μ	Viscosity [mPa · s]
R	Principal radii
A	Apparatus constant [-]
T	Oscillation Period [-]
B	Atmospheric Pressure [mmHg]
V	Volume [cm^3]
d	Diameter of Needle [mm]

Table of Content

1 Introduction

Fossil fuels supplies more than 85 % of the world's energy today [1]. The need for energy will undoubtedly increase with increasing population in the coming years, and consequently the need for energy resources will increase. Petroleum is by far the most utilized energy resource in the world today. In order to meet these demands, new technologies and research is needed. One way of meeting these demands is through optimizing the production of petroleum.

Oil recovery can be divided into three phases, namely primary, secondary and tertiary recovery. Primary recovery is recovery driven by the natural energy drive available in the reservoir. Secondary recovery is promoted by injection of gas and/or water, where injection of water is commonly referred to as waterflooding. After primary and secondary recovery, approximately 60-70% of the oil is left behind in the reservoir. Tertiary recovery, commonly referred to as enhanced oil recovery (EOR), is recovery by chemical-, thermal-, gas-, and microbial injection. [1-2] Another term that is widely used is improved oil recovery (IOR), which refers to any reservoir process that improves oil recovery [1]. Over the last decades, injection of low salinity water to improve oil recovery has been of interest in both laboratories and field [3]. The use of low salinity injection water has increased recovery compared to high salinity/seawater flooding [4][5]. Numerous investigations into understanding this effect have been performed, but the underlying mechanisms are still debated [1-5].

1.1 Objective of Thesis

Understanding how the water and oil chemistry affects the final recovery from a physiochemical standpoint is necessary in order to optimize waterflooding and chemical injection [6]. The main objective of this thesis is a physical-chemical investigation of the crude oil/brine/reservoir rock (COBR) system, and correlation with crude oil composition. Three different crude oils from the North Sea will be investigated. Interfacial tension, zeta potential and contact angle are the main physical-chemical properties that will be investigated to study the COBR system.

2 Background

2.1 Crude Oil, Brine and Solid Phase

2.1.1 Crude Oil

Crude oil is a complex and naturally occurring material, consisting of thousands of individual compounds. Crude oil predominantly consists of hydrocarbons in various molecular structures, and may include heteroatoms commonly known as NSOs (nitrogen, sulphur and oxygen), and small amounts of metals and ions. The composition of crude oils can vary greatly depending on many factors, like geological location and age of the oil fields. These variations arises from different biomass precursors for crude oil and different reservoir conditions like temperature and pressure. [7]

Characterization

The complexity of crude oils makes them difficult to identify by standard techniques, instead they are characterized by dividing the components into a few groups based on their physical and chemical properties. A standard fractionating procedure is the SARA fractionation, where crude oil is separated into Saturates, Aromatics, Resins and Asphaltenes [8-10]. Resins and asphaltenes make up the heavier fractions, consisting of large polar molecules with ill-defined structures. [7]. They are both operationally defined, based on their solubility. The asphaltene fraction, unlike the resin fraction, cannot be dissolved in low boiling liquid hydrocarbons such as hexane and heptane.[10] The asphaltene fraction is thus precipitated from the crude oil based on solubility, and the remaining fractions are separated chromatographically based on polarity in the polarity order resins > aromatics > saturates. [7-8]

In petroleum technology, API gravity (American Petroleum Institute) is commonly used to express liquid density, and is calculated from:

$$API = \frac{141.5}{SP} - 131.5 \qquad \textit{Equation 2.1}$$

Where *SP* stands for specific gravity. The specific gravity of the liquid is that relative to water at 15.6 ºC, and is a dimensionless number. API gravity is customarily expressed in units of degrees, [º]. Oils having API gravity >31.1º are classified as light oils, 22.3-31.1º are medium oils and <22.3º are heavy oils. [7][11] API gravity is thus inversely proportional to density. API gravity of 22.3º corresponds to a density of 0.920 g/cm^3. [7][12]

Viscosity is a measure of a liquids resistance to flow. The viscosity of a liquid relates directly to its intermolecular interactions and molecular structures. Large molecules increases the viscosity of oils, due to both molecular entanglements and increased London-force interactions. Heteroatoms produce permanent dipoles in molecules, which increases intermolecular interactions and consequently increases viscosity. Liquids that have high viscosities tends to be high-density. Viscosity is also highly temperature dependant, and decreases with increasing temperature. [7] Conventional crude oils are characterized as Newtonian fluids [13]. Newtonian means that the viscosity is independent on shear rate [14].

Total acid number (TAN) is a measure of a crude oils acidity [15]. TAN is expressed in milligrams of potassium hydroxide needed to neutralize the acid in one gram of oil [16]. Likewise, total base number (TBN) is a measure of a crude oils basicity [15].

Polar Components

The polar molecules in the crude oil are amphiphilic. Amphiphilic means that the molecule consists of one hydrophobic and one hydrophilic end. Such molecules are commonly referred to as surfactants. Surfactants are surface-active compounds that spontaneously adsorbs on surfaces and interfaces, in order to satisfy the solubility characteristic of both the hydrophobic and hydrophilic end. [17] The hydrophilic end can include alcohols, ethers, NSOs, or acidic or basic functional groups [9-10, 18-19].

Asphaltenes and resins are the most polar components in crude oil [7, 8-10]. Naphthenic acids are a common class of crude oil surface-active species, found in the resin fraction [20]. Naphthenic acids is a collective term for all carboxylic acids present in crude oil, including acyclic and aromatic acids [15]. Presence of any basic species in the crude oil also contributes to surface-activity [9-10, 15, 18-19, 21]. Barth et al. [21] have reported a strong correlation between asphaltene content and TBN by investigation of twenty different crude oils. However, they concluded that the asphaltene fractions are not in themselves bases.

Biodegradation

Crude oils can be subject to biodegradation, which is a microbial alteration of the crude oil [8]. Saturated hydrocarbons are normally degraded first, concentrating heavy polar and asphaltene components in the crude oil [8, 18]. Biodegradation results in reduction of the crude oil quality, by increasing its density, viscosity, TAN, asphaltene and sulphur content, among other [7-8, 18].

2.1.2 Brine and Solid Phase

The brine phase is the aqueous phase in a COBR system. The brine phase can be varied with regard to salinity, ionic strength and pH. Different salts are used to adjust salinity. Particularly, monovalent (e.g. Na^+) versus divalent (e.g. Ca^{2+}) cations can have different effects on the COBR system.

The main component of reservoir sandstone are silica (SiO_2) [22-23]. When silica come into contact with aqueous solutions, the surface is hydrolysed and generates silanol groups (SiOH) [24]. The silica surface charge is dependent on the pH of the aqueous solution, a high pH will generate a negative charge (Equation 2.2) and a low pH will generate a positive charge (Equation 2.3 and 2.4) [25]:

$$Si-OH+OH^- \leftrightarrow Si-O^- + H_2O \qquad \textit{Equation 2.2}$$

$$Si-OH+H^+ \leftrightarrow Si-OH_2^+ \qquad \textit{Equation 2.3}$$

$$Si-OH+H^+ \leftrightarrow Si^+ + H_2O \qquad \textit{Equation 2.4}$$

2.2 Interfacial Tension

For two immiscible liquids, the molecules of each bulk phase prefers to stay together, rather than mix [26]. The molecules at the interface will thus experience an inward-pull due to intermolecular forces [17]. At a molecular level, interfacial tension (IFT) results from the difference in energy between molecules at a fluid interface compared to the corresponding bulk molecules [26]. Interfacial tension is also correctly defined as measure of how much mechanical energy that is required to create a new unit area between two immiscible fluids [26][17].

The Young-Laplace equation relates the capillary pressure ΔP across an interface, with the curvature of the interface and the interfacial tension γ [26]:

$$\Delta P = \gamma\left(\frac{1}{R_1} + \frac{1}{R_2}\right) \qquad \textit{Equation 2.5}$$

Where R_1 and R_2 are the principal radii of curvature of the drop [17]. Capillary pressure is the difference in pressure between two fluids, measured at the interface between the two fluids [27], and is directly proportional to the curvature of the interface [17].

2.2.1 Interfacial Tension in the crude oil/brine system

As mentioned earlier, crude oil contains surface-active compounds, which can readily interact with the brine phase. The IFT of the crude oil/brine (COB) system is thereby dependent on the composition of both the crude oil and the brine. [6, 19, 28-33]

The surface-active molecules in the COB system makes the IFT measurements time-dependant [6, 19, 28-34]. When the phases come into contact, the IFT falls steadily into an equilibrium value. The decline rate is dependent on molecular diffusion and reorganization, and adsorption/desorption processes. [29-30] The time it takes for the system to reach equilibrium may vary from seconds to several hours. When the brine phase has a high pH, a monotonic decline is not necessarily the case. The IFT normally decrease rapidly and then increase again, creating a tension minima [30].

Various attempts have been made to correlate the crude oil composition to IFT. Buckley et al. [28] [33] used a linear multivariate statistical analysis to correlate crude oil properties and IFT for 42 different crude oils. They reported that IFT is strongly dependent on brine pH, particularly they observed a considerable decrease in IFT at high pH. At low brine pH, they

found that IFT decreased with increasing TAN. At low pH, they also found that IFT increased with increasing crude oil viscosity. At neutral to medium high brine pH, they found that IFT increased with increasing TBN. At pH above 10, they reported that ultralow IFT was only measurable if TAN was below 0.1 mg KOH/g oil. At all brine conditions, they reported that IFT increases with increasing asphaltene content. The increase in IFT with increasing asphaltene content showed greatest effect at pH 6. They reported that crude oil viscosity was correlated with IFT only if TAN was included, which indicates that some acidic species associate with each other in the oil and thus exert influence on viscosity rather than on IFT. They found no correlations between IFT and density or iso-electric points.

Varadaraj et al. [31] investigated the IFT of the asphaltene fraction, and the deasphalted oil, of five different heavy crude oils. They added the asphaltene to the deasphalted oil, and observed a decrease in IFT with increasing asphaltene concentration. They suggested that an interaction between crude oil naphthenic acids and asphaltenes leads to high interfacial activity for crude oils [31-32]. Varadaraj et al.[32] later reported that crude oil naphthenic acids are more effective than crude oil asphaltenes in reducing IFT.

The structure of the crude oil acids may be important for interfacial activity in the COB system. Acevedo et al. [34] reported that crude oil acids of low molecular weight and highly aliphatic structure adsorbed on the COB interface clearly reduced the IFT for Cerro Negro crude oil. They also reported that the heavier acids and asphaltenes probably adsorbed at the interface, contributing to emulsion stability. Varadaraj et al. [32] investigated three different crude oils, and reported that naphthenic acids of low molecular weight were more interfacially active than naphthenic acids of higher molecular weight. They explained that lower molecular weight acids are less soluble in the hydrocarbon phase and thus favour interfacial aggregation. They found that primary naphthenic acids are more interfacially active than secondary and tertiary naphthenic acids. Primary naphthenic acid means that the carbon in the carboxylic acid group is bonded to only one other carbon atom. Secondary and tertiary means that the carboxylic acid group is bonded to two and three carbon atoms respectively. [35] Primary acids are less sterically hindered and exhibit a favourable interfacial packing at the surface [32].

Brine salinity and composition have great influence on IFT measurements [6, 19, 28-30, 33]. Alotabi et al. [6] reported that lowering the NaCl concentration increased the IFT. Poteau et al. [19] investigated the asphaltene fraction of a Venezuelan heavy crude oil and reported that pH has a strong influence on the interfacial properties of asphaltenes at the COB interface. At high

and low pH, the functional groups of the asphaltene fraction become charged. Charging the functional groups of the asphaltene fraction yields a more hydrophilic behaviour and enhances surface activity. They reported that the effect is strongest at high pH, because asphaltenes contain more acidic than basic groups.

Presence of Ca^{2+} ions in the brine phase may affect the IFT of the COB interface. Tichelkamp et al. [36] explained that calcium ions can form 1:2 ion pairs with dissociated naphthenic acids, which can reduce the IFT. This calcium(1):(2)dissociated acid complex will have a higher oil solubility and can thus migrate into the oil phase, consequently reducing interfacial activity. This is in contrast to sodium ions who can only form 1:1 ion pairs, which makes it possible for such components to migrate to the water phase. [36-37]

2.3 Electrical Properties

2.3.1 Electrical Double Layer

When a charged particle is present in a solution containing an excess of ions, the ions will locate themselves around the particle in order to neutralize the surface charge. This accumulation of ions in named the electrical double layer. The electrical double layer consists of two layers – an inner layer, and an outer layer. The inner layer, also named Stern layer, is formed by ions of opposite charge to the particle surface. These ions are named counter ions, and is adsorbed onto the particle surface. The outer layer is a diffuse layer consisting of free ions that move under the influence of electrostatic attraction to the surface charge, and consists of both counter ions and co ions – ions of same charge as the surface. [17][38-39] The electrical double layer is illustrated in figure 2.1:

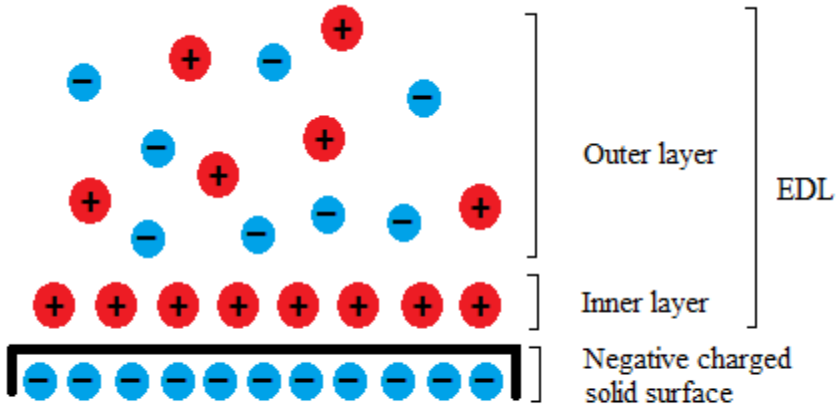

Figure 2.1. Schematic illustration of the electrical double layer for a negatively charged surface.

The thickness of the electrical double layer is called the Debye length, κ^{-1}[nm], and can be expressed by equation 2.6 for electrolyte solutions at 25ºC: [17][38]

$$\kappa^{-1} = \frac{0.304}{\sqrt{I}} \qquad \textit{Equation 2.6}$$

Where I is the ionic strength of the solution, given by:

$$I = \frac{1}{2}\sum z_i^2 C_i \qquad \textit{Equation 2.7}$$

Where z is the ion valance, and C is the molarities of the ions in the solution [17][38]. From equation 2.7, it is clear that the Debye length must decrease with increasing concentration

and/or valance of ions in the solution, and vice versa. This is consistent with the intuitive idea that a higher concentration of ions neutralizes the surface charge within a shorter range, due to more effective screening of the particle surface.

When two charged surfaces approach each other, there will be electrostatic interactions between their electrical double layers. These interactions may be van der Waals attractions and electrostatic repulsion between the double layers. The DLVO theory (after Derjaguin, Landau, Verwey and Overbeek) describes the summing of the attractive and repulsive interactions. DLVO theory is often used to describe the stability of colloids, which are mixtures where one material is dispersed in another. When both the dispersed phase and the medium is liquid, such as oil-in-water, the colloids are referred to as emulsions. [10][17][40] The net interaction potential Φ_{net} between two spherical particles as a function of the distance between them is illustrated in Figure 2.2:

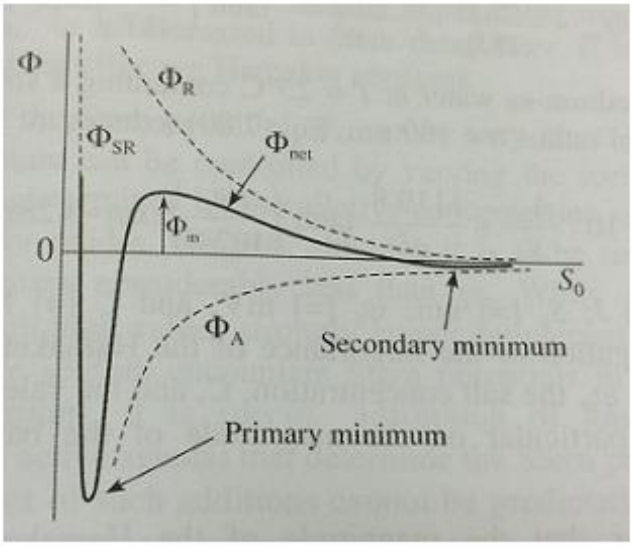

Figure 2.2. The "DLVO curve". Displays interaction potential between two particles. From [17].

Where Φ_R is the repulsion from the double layers, Φ_A is the van der Waals attractions, Φ_{SR} is a short-range repulsion and Φ_m is an intermediate maximum potential representing a 'potential energy barrier'. For an aqueous colloid, aggregation in the primary and secondary minimum is termed coagulation and flocculation, respectively. Coagulation is complete aggregation and flocculation is formation of loose flocks. [17]

2.3.2 Zeta Potential

Located between the inner and outer layer of the electrical doubler layer, is the slip plane. The value of the electrostatic potential at this plane is called the zeta potential. [41] The zeta potential is one of the few measurable parameters that directly describes the EDL [17].

The magnitude of the zeta potential gives an indication of the potential stability of a colloidal system. In the case of this thesis, the colloidal system is droplets of crude oil dispersed in brine. If the dispersed particles have large negative, or large positive, zeta potentials, they tend to repel each other and not flocculate, thus higher colloidal stability. If the particles have low zeta potentials, the particles are not prevented by electrostatic repulsions and tend to flocculate. The dividing line of stable and unstable suspensions is usually taken at + 30 mV or -30 mV. [42] The point where the zeta potential is zero, is denoted the isoelectric point (IEP) [17], and is normally the point where the colloidal system is least stable [42]. At a given particle charge, a larger zeta potential indicates an increased Debye length [39]. Consequently, the zeta potential is a function of salinity.

2.3.3 Zeta Potential in the COBR System

The zeta potential of crude oil droplets dispersed in brine, are dependent on the pH and ionic strength of the brine, and the composition of the crude oil [23, 40, 43-51].

The electric charge on the COB interface mainly arises from the polar components in the crude oil [43, 47-48]. The dissociation of the naphthenic acids on the COB interface leads to a negative electric charge above the acids pK_a [43, 47]. For COB emulsions, the zeta potential generally becomes more negative as pH increases, depending on the polar components in the crude oil and brine composition [40, 43-45]. However, Farooq et al. [51] concluded that specific adsorption of hydroxide ions is an additional source of interfacial charge. They compared the zeta potential of crude oil with and without extraction of acidic components, and found only a small difference in measured zeta potential at elevated pH [51]. At low pH, below the crude oils pK_a, the zeta potential is normally positive due to non-dissociated acids and protonation of basic functional groups [43, 47, 51].

A shift from positive to negative surface charge at low pH, indicates presence of both acidic and basic surface-active groups at the COB interface [43, 49, 51]. At the IEP, the dissociated acid and base groups present at the interface have equal effect on the surface charge. [43] It has

been previously determined that IEP normally occurs at pH ranges from 2 to 6, depending on crude oil composition [43, 46]. The IEP increases with increasing oil base/acid ratio, because of protonation of the basic species at low pH [43, 49].

Presence of calcium ions in the brine leads to a decrease in the magnitude of the zeta potential [52]. A high salinity brine where $CaCl_2$ is the only salt may change the zeta potential to a positive value, also at high pH [51-52]. This is because of an excess of Ca^{2+} ions in the system react with dissociated acid components in crude oil, and form positively charged R-COO-Ca^{+} complexes at the interface [51].

Silica particles dispersed in brine exhibit an electric charge at the brine/silica interface [23, 43, 50-53]. Farooq et al. [23] showed that silica particles have the most negative zeta potential in pure water, and that the magnitude of the negative potential increased as the solution pH increased for both pure water and NaCl-solutions. They found the point of zero charge (PZC) for silica particles in NaCl solution (1500 ppm) to be at pH 3.2 ±0.1. Others have also reported an isoelectric point at pH 2 for silica particles [43, 50]. Buckley et al. [43] reported that the zeta potential of silica particles in NaCl brines became more negative with decreasing salinity. They also reported a significant decrease in the magnitude of the zeta potential for particles that were aged in brine relative to fresh dispersions [43]. Presence of calcium ions reduces the magnitude of the negative zeta potential [23, 50-53]. Farooq et al [23] reported a positive zeta potential around pH 10 due to adsorption of Ca^{2+} ions onto the silica surface, where $CaCl_2$ was the only salt in the brine.

Measurements of the zeta potential for the crude oil/brine and silica/brine system may be used to determine the wettability of the COBR system [23, 40, 43, 50-53]. If they are of the same charge they will repel each other, and the rock will be more water-wet. If they are of opposite charge, there will be an attraction between them and the rock will be more oil-wet. This comes from the stability of the water film between the crude oil and rock, which is a function of the electrical double layer repulsion. High repulsion between the double layers promotes stabilization of a thick water film between the crude oil and rock. [40, 52] This is commonly used to predict wettability for low-salinity waterflooding [50-53], but the effect is less significant for high salinity brines [40, 52].

2.4 Contact Angle and Wettability

Contact angle is a quantitative measurement of liquid-solid interaction, made by a liquid placed against a solid [17]. For this thesis, a system of liquid-liquid-solid interactions will be investigated. The contact angle θ is the angle between the liquid interface and the solid [17], by convention measured in the densest phase [22], see Figure 2.3:

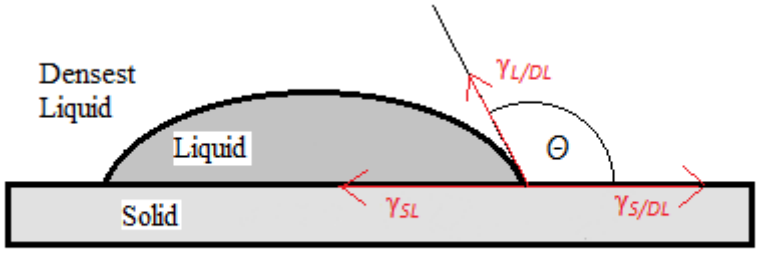

Figure 2.3. Contact angle θ for a liquid-liquid-solid system.

Where γ_{SL}, $\gamma_{L/DL}$ and $\gamma_{S/DL}$ denotes the interfacial tension between solid-liquid, liquid-densest liquid and solid-densest liquid, respectively. The $\gamma_{L/DL}$ is the IFT discussed in section 2.3. In the case of the COBR system, crude oil is the liquid, brine the densest liquid and rock is the solid. By balancing the horizontal forces in Figure 2.3, one can derive at Young's equation [17]:

$$\cos\theta = \frac{\left(\gamma_{S/DL} - \gamma_{SL}\right)}{\gamma_{L/DL}} \qquad \textit{Equation 2.8}$$

Which describes the contact angle for the system in static equilibrium.

Wettability describes the solids preference to be in contact with one fluid, rather than the other [54]. Put in another way; wettability describes the tendency of one fluid to spread on a solid surface in the presence of other immiscible fluids [55]. For the COBR system, if the contact angle is less than 90º the solid phase is water-wet and, if the contact angle is larger than 90º the solid phase is oil-wet. The value of the angle can reflect the strength of a solids wettability by a fluid. Arbitrarily wettability classes has been suggested; between 0-30º, strongly water wet; 30-90º, preferentially water-wet; 90º, neutral wettability; 90-150º, preferentially oil-wet, and 150-180º, strongly oil-wet. [55][22]

Silica surfaces are typically water-wet. The surface of such a water-wet solid is coated by a film of the water phase. The part of this water film that is closest to the solid surface forms an electric double layer (will be explained in section 2.5), where the solid surface charge are countered by ions in the water phase. Such an electrical double layer will also be formed at the water-oil

interface. When these interfaces are in proximity, attractive and repulsive forces will come in to play. There will be attraction if the interfaces have opposite charges, and repulsion if they are of the same charge. A destabilization of the water film allows polar components in the oil to adsorb onto the surface, making it less water-wet or even oil-wet. [3, 54]

2.4.1 Contact Angle in the COBR system

The contact angle in a COBR system is dependent on the interactions between all the three phases, and consequently on their compositions.

At a given brine salinity, different pH can lead to destabilization of the water film. Silica surfaces are negatively charged above a pH of 2. [54] When the brine phase has a low pH, basic species in the crude oil is protonated and the COB interface assumes a positive charge. When the pH of the brine phase increases, naphthenic acids starts to dissociate and the COB interface achieves a negative charge. [57].

If a rock surface is contacted by crude oil, the potential exists for adsorption of water-insoluble polar components from the crude oil [43]. An initially water-wet rock surface can be altered by adsorption of polar compounds in the crude oil, particularly the acid and basic components from the asphaltene/resin fractions [3]. There is a destabilization of the water film due to attraction between the phases, which further allows for adsorption of the polar components on the water film [3, 54].

Buckley et al. [57] identified four mechanism of interaction between silica surfaces and crude oils. (1) Polar interactions that predominate in the absence of water film. (2) Surface precipitation depending on the crude oils solvent properties with respect to asphaltenes. (3) Acid/base interactions in the presence of water. (4) Ion binding or specific interactions between charged sites and higher valency ions.

Buckley et al. [57] compared wettability of several crude oils on glass surfaces. They found that the combination of acid number, base number and API gravity can give an indication to which extent an oil will alter wetting. They suggested that crude oils of increasing API gravity showed decreasing solvent properties for their asphaltenes. They found that wetting alteration was greatest for Lagrave and Moutray crude oil. Lagrave has relatively low acid and base number, but the highest API gravity. Moutray has a high acid number and low base number, and a lower API gravity. This indicate that Lagrave depends on precipitation, and Moutray

dependes ion binding, for wettability alteration. They also concluded that a high acid content yields a high negative surface charge, which likely promotes interaction with Ca^{2+} ions.

Dissolved divalent ions, such as Ca^{2+} can destabilize the water film [54]. That is because these divalent cations can form a bridge between the negatively charged solid and components at the COB interface [56]. This means that the presence of Ca^{2+} ions can lead to a wettability alteration towards oil-wet [3]. Presence of Ca^{2+} can interact in several ways: oil-Ca-oil, mineral-Ca-mineral, and oil-Ca-mineral. The first two can limit wettability alteration, whereas the last can promote wettability alteration. The limiting of alteration arises because of the cations ability to bridge the two negatively charged surfaces [3, 54, 56-57].

Nasrella et al. [46] concluded that low salinity brines resulted in more water-wet surfaces, and high-salinity brines produced high contact angles. Yang et al. [56] also reported that increased salinity appeared to result in closer approach between the rock and oil due to decreased electrostatic repulsion, and thereby a less water-wet system.

2.5 Low Salinity Waterflooding

Low salinity waterflooding has been proven by many to improve oil recovery [1-2, 4, 6, 58-65]. However, there is no consensus on a particular dominant mechanism that explains the low-salinity effect [1-2, 4, 6, 60]. The potential for improving oil recovery by injection of low salinity water in sandstone reservoir is of interest because of relatively low cost and environmental aspects [46].

It is widely accepted that a presence of clay minerals and polar components in the crude oil are important to observe any low-salinity effect [60, 63-65]. However, the effect of presence of acids, bases and asphaltenes is not fully understood [60]. Alotabi et al. [6] explained that the low salinity effects arises from the wettability of the reservoir. They explained that the low salinity water expands the EDL, which alters the wettability towards water-wet. Wettability is strongly dependant on the oil composition, surface chemistry of the rock and aqueous phase [6]. McGuire et al. [62] proposed mechanism similar to alkaline flooding: generation of surfactants, wettability alteration and reduction in IFT. They explained that injection of low salinity water generated hydroxide ions through reactions with reservoir mineral, which elevates the pH. Lager et al. [63] reported that cation exchange between the mineral surface and the invading brine is the primary mechanism for improved recovery by low salinity flooding. However, Sandengen et al. [61] reported core flooding results where injection of low salinity water yielded more oil-wet conditions, and utilized the ion exchange mechanism to explain that low salinity waterflooding can alter wettability both ways.

3 Method

3.1 Crude Oil and Brine Preparations

3.1.1 Crude Oil Preparations

Three different crude oils were used in this thesis, denoted here as crude oil A, B, and C. The crude oils originated from three different fields in the North Sea, and were provided by Statoil ASA.

Before every measurement that was conducted in this thesis, the crude oils was homogenized by heating before sampling. The flask containing the crude oil was set in a water bath for 1 hour, at a temperature of 60ºC. The lid of the container was opened slightly during heating, to avoid a pressure build-up. The container was shaken 2-3 times during heating, to ensure homogenization of the oil.

3.1.2 Preparation of Brines

The brines were prepared by weighing in the amount of salt, and mixing with distilled water. The brines were left to stir for 1-2 hours, until all the salt was dissolved. The salts used was NaCl (Sigma Aldrich, 99.8% purity) and $CaCl_2 \cdot 2H_2O$ (Sigma Aldrich, 99% purity). pH was adjusted with addition of 1 M HCl and NaOH (both chemicals from Sigma Aldrich, 98.0% purity). The stated pH-values have an uncertainty of ±0.2. The pH was measured using a Metrohm pH-meter equipped with a Cl-Ag electrode.

3.1.3 Source of Error

The intention was to have one low-salinity (0.03 M) and one high-salinity (0.60 M) brine with NaCl, partly to study the effects of an expanded/compressed electrical double layer in the COB/COBR systems. In addition, one low-salinity brine (ionic strength 0.03 M) with presence of Ca^{2+} ions was prepared. The calcium brine was prepared with a mole fraction of 0.04 calcium ions relative to sodium ions ($X_{Ca/Na} = 0.04$). Due to a calculation error, the NaCl brines were made with a four times higher concentration, namely 0.12 M and 2.40 M, which represents a medium-salinity and a high-salinity brine. The Debye length as a function of electrolyte molar concentration is illustrated in Figure 3.1 [17]:

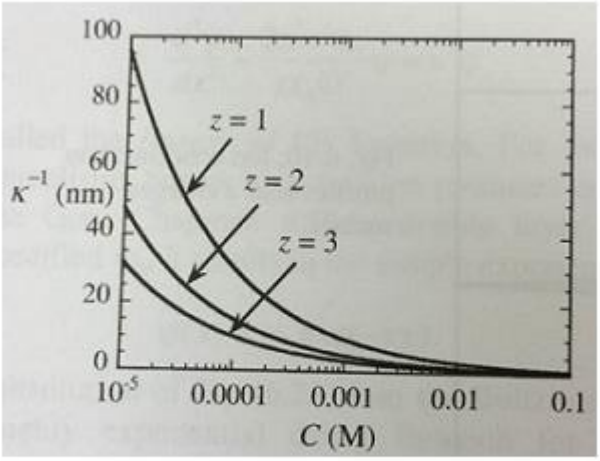

Figure 3.1. Displays the Debye length (κ^{-1}) as a function of electrolyte molar concentration. From [17].

From Figure 3.1, it can be observed that the Debye length is close to zero when the electrolyte concentration is 0.1 M. This further makes it reasonable to assume that the EDL of particles dispersed in a brine with an electrolyte concentration of 2.40 M is practically non-existing. Consequently, any effect of EDL with these two concentrations (0.12 M and 2.40 M) is not expected to be significant. One objective of this thesis was to investigate any effects of low versus high salinity, and also to investigate any effects of calcium ions at same ionic strength. A low salinity brine of 0.03 M NaCl concentration was therefore prepared later, and measurements with this brine were thus conducted at a later stage. Due to both limitation of time and unexpected results, the 0.03 M brine was not used in measurements of contact angles.

The error in salinity was discovered after all measurements had been conducted. They were discovered by investigation of the zeta potential results. One reason for this discovery was that '0.03 M' brine (really the 0.12 M brine) showed considerably higher conductivity than the brine of same ionic strength that contained calcium ions. In addition, the presence of calcium ions appeared to increase the magnitude of the zeta potential drastically, which was not expected. As these results were unexplainable, it was eventually found that the NaCl were in fact four times more concentrated than intended (i.e. 0.12 M and 2.40 M instead of 0.03 M and 0.60 M, respectively).

3.2 Density Measurements

3.2.1 The Oscillating U-Tube Method

The oscillating U-tube method [66] is used to measure density in this thesis. The method obtains the liquid density of a sample based on electronic measurements of the natural vibrating frequency of a hollow U-tube containing the investigated liquid. The oscillating frequency of the tube is dependent on the mass of the tube, which consequently makes the frequency a function of the density of the liquid. The density meter measures the oscillators' period *T*, which depends on the samples density by the following equation:

$$\rho = A\left(T^2 - T_0^2\right) + \rho_0 \qquad \textit{Equation 3.1}$$

Where ρ and ρ_0 is the density, and T and T_0 is the period of the sample and solvent respectively, and A is the apparatus constant. [67] The apparatus constant can be found by conducting calibration measurements of samples with known densities, air and water are commonly used. The density of water at 293 K is 0.997 g/cm^3 [68]. The density of air can be calculated by the following equation [67]:

$$\rho_{air} = 0.046464 \cdot \frac{B - F \cdot 0.08987}{T} \cdot 10^{-3} \qquad \textit{Equation 3.2}$$

Where B is the atmospheric pressure in mm Hg, F is the relative humidity in %, and T is the temperature in Kelvin. Once the apparatus constant A have been decided, Equation 3.1 can be used to calculate the density of the sample.

3.2.2 Experimental Procedure

The density of the crude oils was measured using a DMA 60 density meter from Anton Paar, equipped with a DMA 602 hollow glass U-tube that holds 1 mL of fluid. The glass tube is placed inside a stainless steel tube, which is connected to a water bath to maintain a constant temperature.

The samples were injected continuously into the glass U-tube by a syringe, until no air bubbles were visible in the tube. Water/air was measured first, to determine the apparatus constant (Equation 3.1). The crude oil samples was then measured in the same way, Equation 3.1 and 3.2 was used to determine the densities.

3.3 Viscosity Measurements

A rotational rheometer (Kinexus Pro from Malvern Instruments Ltd.) is used to measure viscosity in this thesis. The rheometer applies a controlled shear deformation to the crude oil samples by a rotating spindle, measuring its flow properties. The setup is shown in Figure 3.2:

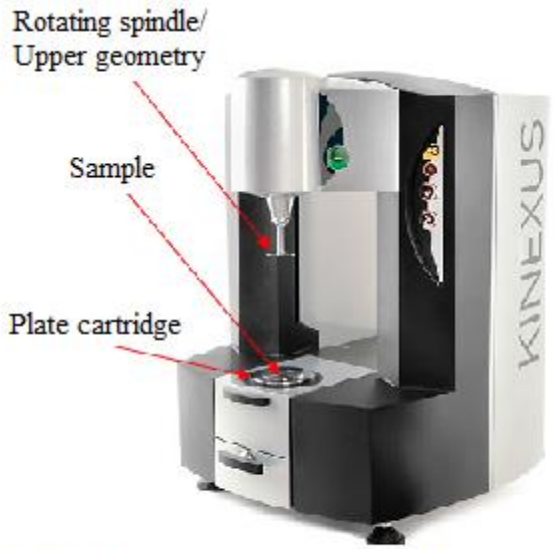

Figure 3.2. Setup for measurement of viscosity, using a rotational rheometer. Picture adapted from [78].

The crude oil sample was placed in the middle of the plate cartridge. The upper geometry was then lowered down onto the sample. Any visible oil on the side of the geometry was wiped away before conducting the measurements. Crude oils are ideally Newtonian fluids, the measurements were thus conducted at a constant shear rate of 10 s^{-1}. All measurements were performed at constant temperature of 25ºC.

Only one parallel is measured for each crude oil sample. It is assumed that the measurements have an uncertainty of 5 %.

3.4 Interfacial Tension

3.4.1 Pendant Drop Method

The Pendant Drop Method is utilized for measurements of IFT. Pendant Drop determines the profile of a drop hanging from a needle. The shape of the drop is dependent on the gravitation force, that elongates the drop, and surface tension that holds the drop in a spherical form to minimize surface area. The curvature of the drop is characteristic for the equilibrium state, which is defined mathematically by the Young-Laplace equation (Equation 2.5). The IFT can be calculated if the drop is sufficiently large so that the shape differs significantly from a spherical form. [69] The drop shape parameter is a dimensionless drop profile, which gives the relationship between the gravitational force and the surface tension, and can thus be used as a quality parameter for the measurements. [17][26][69]

3.4.2 Equipment

IFT measurements were carried out on the OCA20 instrument from DataPhysics. The goniometer utilizes a high-resolution CCD camera connected to a computer equipped with a software that performs analysis of the drop shape [69]. The goniometer has an automatically controlled piston that holds the syringe to control drop-volume and a homogenous light source. Picture of the setup is shown in Figure 3.3:

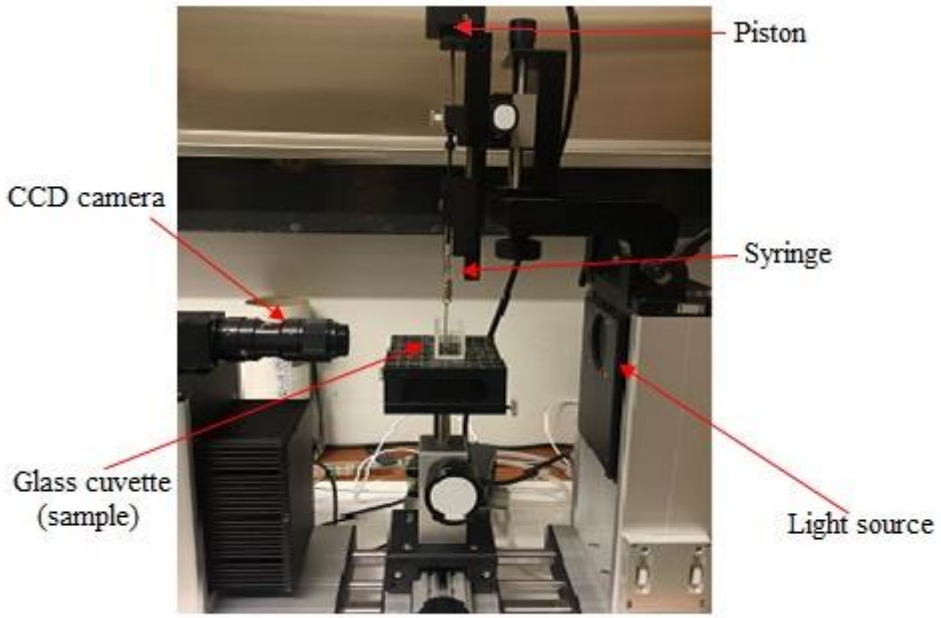

Figure 3.3. Setup for IFT measurements.

Because the drop phase (crude oil) is less dense than the surrounding phase (brine), an inverted needle is necessary to conduct the measurements. The diameter of the needle is varied within a range of 0.30 mm – 2.05 mm, and connected to a 500 µL –Hamilton syringe. The brine is contained in a glass cuvette made from optical glass.

3.4.3 Experimental Procedure

After homogenizing the crude oil by heating, the syringe was rinsed three times with the oil before filling it with sample. Because the sample volume is so small, it is assumed that the temperature of the crude oil will go to room temperature rapidly, there was approximately a 5-minute wait between sampling and measurements. In this thesis, the crude oils have not been pre-equilibrated with brine prior to measurements, as pre-equilibration does not eliminate changes with time [33]. The outside of the needle was washed with DCM:methanol (93:7, v/v) prior to immerging it into the brine phase. The washing of the needle is particularly important to avoid any organic residues on the needle, as this would lead to the drop falling down because of a higher affinity towards the needle.

Before starting the actual measurements, 1-2 test runs were conducted in order to decide ideal needle diameter and drop volume. Both needle diameter and drop volume were decided based on the value of the shape parameter. The criterion was that the shape parameter should lie between 0.45 – 0.75 and ideally at 0.6.

Ideally, the crude oil/brine should be in equilibrium when the IFT is decided. The IFT is considered to be in equilibrium when plotting the IFT as a function of time yields a horizontal slope. See Figure 3.4:

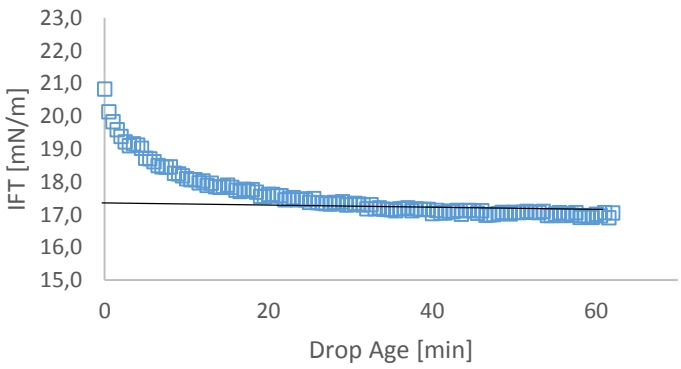

Figure 3.4. Shows IFT as function of drop age. Slope is horizontal after approximately 40 minutes and thus considered to be in equilibrium.

The time it takes for the IFT to reach equilibrium varies greatly with crude oil and brine composition. From initial test runs, it was observed that the time it took for equilibrium to be reached in the crude oil/brine system varied between a few minutes to several hours. Based on several measurements over different timescales it was decided to use a 1-hour experimental run for all samples, focusing on applying a systematic method for all samples. After the 1-hour experimental run, the IFT value is taken directly. These are the reported IFT values in this thesis. During the 1-hour experimental run, a measurement is conducted automatically every 30 seconds.

In the cases where the measured IFT values were below 6 mN/m at elevated pH, a 1-hour experimental run was not feasible due to unstable droplets. The droplets either detached from the needle (Figure 3.5(a)), slid down the needle (Figure 3.5(b)), or assumed a spherical shape (Figure 3.5(c)) during the measurements:

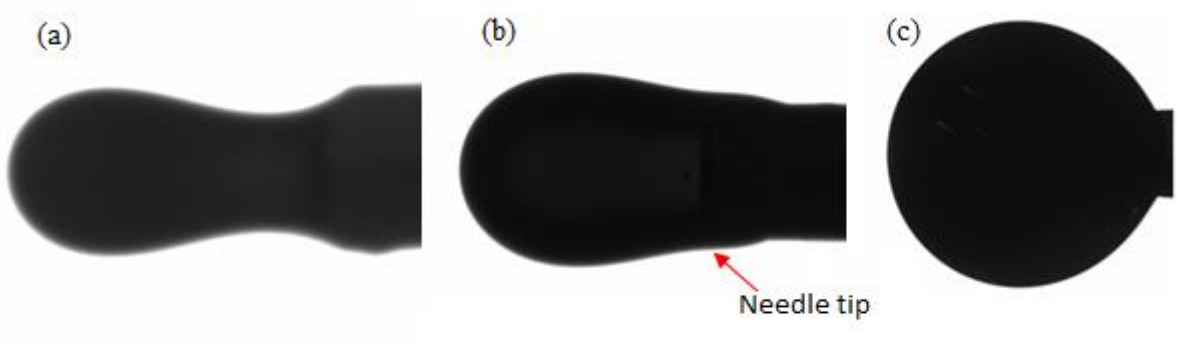

Figure 3.5. Picture of droplet (a) detaching from the needle, (b) sliding down the needle and (c) pulling back into a spherical shape.

The reported values for these measurements are thus obtained after shorter experimental runs, in the range of 3 to 10 minutes. The same shape parameter criterion is valid for these measurements.

Prior to IFT measurements of the crude oils, the IFT of a decane droplet in distilled water was measured, in order to validate the method. The measured IFT was compared to literature value, where Goebel et al. [77] reported the IFT of decane/water to be 53.2 mN/m.

Before, after an in between each different measurement, the needle, syringe and glass cuvette is washed. They are first washed three times with toluene, then three times with ethanol, and lastly three times with distilled water.

Standard deviations are calculated from five parallels at one condition, for each crude oil.

3.4.4 Source of Error

In the cases where the IFT is too low to form a stable drop, the IFT is not reported. In these cases the crude oil was continuously dispensed out of the needle, but the phases were still immiscible. The IFT could probably be measureable with other techniques, such as the spinning drop method [17][33], however, such measurements were beyond the scope of this work.

For low and neutral pH, and in some cases weakly basic pH, the shape parameter was usually below 0.6. This is because larger drop volumes caused the drop to detach from the needle before a 1-hour run was completed. Lower shape parameters makes the mathematical approximation of the interfacial tension less exact, which can indicate that there are uncertainties connected with the results.

The glass cuvette used for containing the brine phase is approximately 2 cm high. This limits how large the crude oil drop volume can be. This again puts limitations to the shape parameter, and consequently the quality of the IFT measurements.

The IFT is dependent on the density difference between the crude oil and brine phase. The densities of the brine phases has not been measured in this thesis, and the density of pure water at room temperature has been set as brine density. The IFT can be modelled as displayed by the Harkins and Brown equation [70]:

$$\gamma = \frac{V\Delta\rho g}{d\pi F} \qquad \textit{Equation 3.3}$$

Where V is the volume of the drop, $\Delta\rho$ is the density difference between the two phases, g is the gravitational constant, d is the needle diameter and F is a dimensionless empirical correlation-constant fitted by the drop shape analyser [70]. From this equation, we see that the density difference is proportional to the IFT. The right IFT value could be found by simply multiplying by a small factor. A quantitative comparison between the different crude oils should thus be valid. The difference in density for a 0.03 M and 2.40 M NaCl solution is less than 0.1 g/cm^3. Which is smaller than IFT standard deviations. Thus, comparison between the different salinities should also be valid.

The measurements are sensitive to vibrations. Noise within close proximity of the instrument visibly caused vibrations of the drop, which caused jumps in the IFT results. The drop quickly settled after being subjected to vibrations, so that these jumps are seen in one single measurement point. In these cases, such jumps are removed from the measurements series.

3.5 Zeta Potential

3.5.1 Equipment

Zetasizer Nano ZS from Malvern Instruments Ltd. was used to measure the zeta potentials of crude oil emulsions.

The sample is injected into a capillary cell that have electrodes at both ends, see Figure 3.6:

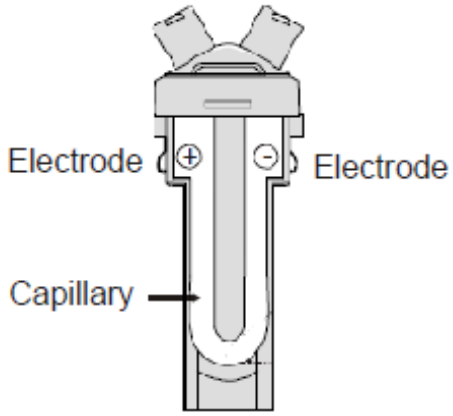

Figure 3.6. Capillary cell for zeta potential measurements. Adapted from [71].

An electric field is applied across the sample, which causes the charged particles to migrate towards the electrode of opposite charge. This eventually leads the particles to move with constant velocity, commonly referred to as its electrophoretic mobility (U_E). Zeta potential is obtained from the electrophoretic mobility by applying the Henry equation:

$$U_E = \frac{2\varepsilon\zeta f(ka)}{3\eta} \qquad \textit{Equation 3.4}$$

Where ζ is the zeta potential, ε is the dielectric constant, η is the viscosity and *f(ka)* is Henry's function. [71] The Smoluchowski approximation of Henry's function is used for the work in this thesis.

3.5.2 Sample Preparation and Measurement Procedure

The procedure used for measurements of zeta potential, is written by Christer Llano Andresen [72]. 10 mL of brine and 5 µL of crude oil is added to a glass container, shaken by hand until they are visibly mixed, and the submerged into an ultrasonic bath for 5 minutes. This is in order to create emulsions. The sample is then immediately injected into the capillary cell with a

syringe. The cell was held up-side-down during injection until it was half-full, and then turned back for further injection, in order to avoid air bubbles in the cell. Lastly, the cell was inserted in the Zetasizer.

The following configurations were used:

- Sample: Polystyrene latex cell.
- Dispersant: Temperature 25 ºC, viscosity 0.8872 CP, RI 1.330.
- Temperature: 25.0 ºC, equilibrium time 120 seconds.
- Model: Smoluchowski approximation.
- Cell: Disposable folded capillary cell
- Measurements: minimum 10, maximum 100.
- Analysis Model: Auto Mode.

Three to ten parallels were measured for each sample and within each parallel, a minimum of ten runs is conducted (as set in the configurations). Since the amount of measuring points per parallel is relatively large, it was decided that if one or two parallels were of poor quality, the remaining results would be sufficient to describe zeta potential.

Over time, the electrodes of the capillary cell tended to turn black. This could be due to crude oil accumulating on the electrodes, or it could be worn from the applied voltage. This indicates that the quality of the cells decreases with usage, which could affect the results. To ensure that used cells provided adequate results, the quality of the cells were tested by running a measurement with a zeta standard with a known zeta potential of 42 ± 5 mV.

The zeta cells were washed by flushing them first with distilled water, then ethanol, and lastly distilled water again.

3.5.3 Determining the Zeta Potential and Standard Deviation

The results for the zeta potential measurements are given as a distribution curve in the software. This distribution curve has an associated mean value and standard deviation. When reporting zeta measurements, this mean value represents one parallel.

Calculating the average zeta potential of several parallels is done by simply calculating the average of the mean zeta potential in the different parallels. When calculating the mean standard

deviation for the parallels, the distribution curve needs to be taken into consideration. The standard deviation can be calculated by the following equation [73]:

$$\sigma = \sqrt{\frac{\sum_{i=1}^{n} \sigma_i^2}{n}} \qquad \textit{Equation 3.5}$$

Where σ is the mean standard deviation, σ_i is the standard deviation for each parallel and n is the number of parallels.

This can be illustrated with an example. We have three parallels with associated means X_1, X_2, X_3, and standard deviations σ_1, σ_2, σ_3. The average zeta potential and standard deviation is calculated as follows:

$$\overline{X} = \frac{X_1 + X_2 + X_3}{3} \qquad \sigma = \sqrt{\frac{\sigma_1^2 + \sigma_2^2 + \sigma_3^2}{3}}$$

3.5.4 Source of Error

When the electrophoretic mobility is measured, it is assumed that the dispersed particles are spherical [17][71]. Since crude oil consists of a variety of macromolecular components, it is safe to expect that the particles are in fact non-spherical and that this will influence the results.

Equation 3.4 assumes that there is a linear dependency between electrophoretic mobility and zeta potential [71], which is not necessarily true . The relative standard deviations for both zeta potentials and the electrophoretic mobility were calculated, to check if one result was more accurate than the other. The differences were not significant, so only the values for zeta potentials will be discussed in this thesis.

In some cases, especially for crude oil C in 0.03 M NaCl solution, and often for various measurements at high pH, the software expressed poor distribution data for no obvious reason. Poor distribution data is often the result when a sample concentration is too high or too low, if the conductivity is too high, or if there are too few runs in a measurement [71][74]. As none of these criteria seemed to apply for the conducted measurements, the results were used as long as they did not clearly deviate from the other parallels.

The results from measurements with the 0.12 M NaCl brine did not produce a distribution curve and a corresponding standard deviation, as for the other brines. This was because the analysis

model was set to auto mode, which automatically switched to monomodal analysis for these samples due to high conductivity (above 10 mS/cm) [71]. The standard deviation for these samples are calculated from the parallels, and it is safe to assume that the actual deviation would be considerably higher.

If a sample was shaken 'too much' or 'too little' before exposing it to the ultrasonic bath, the measurement results were poor. In these cases, the zeta potential was measured to be right above or below zero, and at the same time the software expressed that the distribution data was poor. In these cases, new samples was prepared until adequate results were obtainable. The same type of results were observed when trying to conduct measurements at a 2.4 M ionic strength, probably due to too high sample conductivity to obtain good results. It was therefore decided to use the 0.12 M brine as high ionic strength, and 6 mM as the lowest ionic strength for the zeta potential measurements. When the samples are shaken manually before immerging them into the ultrasonic bath, it is difficult to ensure that all samples are handled identically. Consequently, the energy input is probably slightly different for the samples. This could lead higher or lower emulsion stability for the different samples, and consequently a higher or lower zeta potential. The effect is probably not significant, as the energy input from the ultrasonic bath is much higher and equal for all samples.

When preparing many consecutive samples for measurements, the temperature of the ultrasonic bath increases. Consequently, the last samples will have a slightly higher temperature than the first. This could affect the results, considering that oil-in-water emulsion stability decreases with increasing temperature [45]. Lower emulsion stability could lead to lower measured zeta potentials, higher deviation in the measurements, or poor distribution data if the emulsion separates.

3.6 Contact Angle

3.6.1 Sessile Drop Method

The sessile drop method is used for measurements of contact angle in this thesis. A tangent line is placed on the sessile drop profile at the point of contact with the solid surface. The contact angle is measured from this tangent line. [69]

3.6.2 Equipment

The same instrument that was used for IFT measurements, was used for measuring contact angles, namely the OCA20 from DataPhysics.

A glass plate representing the rock phase was imbedded in the experimental setup. The plate is elevated in the glass cuvette by a supportive stand, allowing the crude oil droplet to stick to the glass plate from below. The 0.30 mm diameter inverted needle is used in these measurements. The setup is shown in Figure 3.7:

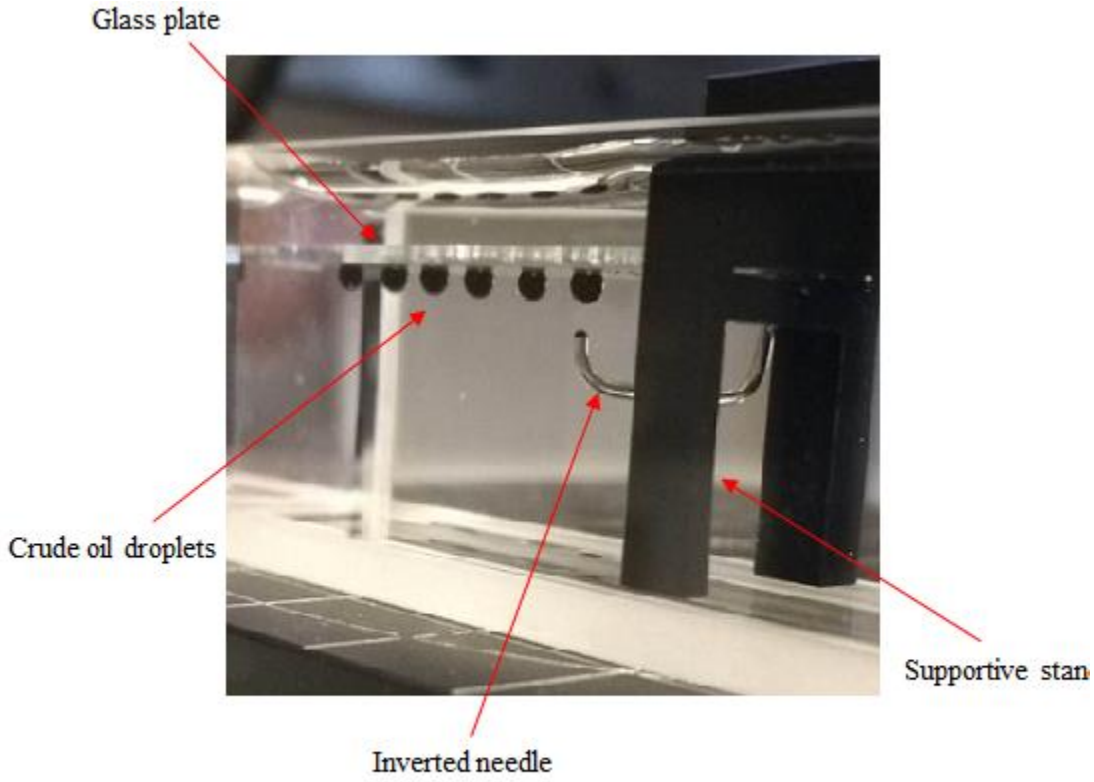

Figure 3.7. Illustration of the experimental setup in contact angle measurements.

3.6.3 Experimental Procedure

Samples were prepared in the same way as the IFT samples; after homogenizing the crude oil by heating, the syringe was rinsed three times with the oil before filling it with sample. Because the sample volume is so small, it is assumed that the temperature of the crude oil will go to room temperature rapidly, there was approximately a 5-minute wait between sampling and measurements.

The dispensed crude oil droplets have a volume of 7 μL. The choice of drop volume is based on literature stating that a drop volume between 1 – 10 μL is preferential for a water/air/solid system [75]. Initial measurements were run for 1 hour to check if the measurements stabilized within this timeframe. It was found that the measurements appeared to stabilize around a 15-20 minute run time, and it was decided that a 20-minute experimental run would be used for all measurements. The value for the contact angle is taken directly after 20 minutes. During the 20-minute experimental run, a measurement is conducted automatically every 30 seconds. The contact angle reported here is the average between the left and right contact angles.

The glass cuvette, needle, syringe and supportive stand was washed as described for IFT measurements. The glass plates were rinsed with toluene, ethanol and distilled water after usage. They were then transferred to an alkaline bath, and left for 24 hours. The alkaline bath is made from water mixed with the detergent Sodosil, until it reached pH of about 9. The glass plates were then rinsed thoroughly with distilled water.

3.6.4 Source of Error

It was intended to run a full measurement set with decane as the oil phase, in order to observe the effect in contact angles for an oil that did not contain any surface-active species. Due to limitations of both time and usable glass plates, a full set was not obtained. It was also intended to measure the contact angles of brine droplets on the glass plates, to compare the effects with the crude oil contact angles. However, the water droplets evaporated before a full 20-minute run could be performed and thus had to be measured upon contact. The results from these measurements were difficult to interpret in correlation with the crude oil measurements, and are therefore not reported in this thesis.

Measurements at high pH for NaCl brines were difficult to conduct. The crude oil droplets appeared to spread over the glass plates, and sometimes slid off. This is explained in more detail

under section 5.3. It would perhaps be useful to measure contact angles around pH 8, as pH 9 proved to be difficult to measure with this procedure.

If the glass plates are contaminated with organic impurities, this could lead to the crude oil droplets having a higher affinity towards the glass plates. To check if the plates were clean, a drop of water was placed on the plate to make sure that it spread. This could have been done more accurately by measuring the contact angle and comparing it to literature values.

It was discovered that leaving the glass plates in a Sodosil-bath for several days resulted in a highly hydrophilic surface. The surface maintained a highly hydrophilic character even though large amounts of distilled water was used for rinsing. This could indicate that using Sodosil for washing the glass plates may not be ideal, even for 24 hours. This was, however, not discovered until all crude oil measurements had been conducted. It could thus be useful to test another washing procedure, for instance to use an ultrasonic bath and hydrogen peroxide, used by Buckley et al. [57].

4 Results

4.1 Physical and Chemical Properties

The measured densities and viscosities for the crude oils are listed in Table 4.1. TAN, asphaltene content and degree of biodegradation are provided by Sørbø [76], also listed in Table 4.1.

Table 4.1. Lists measured density and viscosity of crude oil A, B and C. Values for TAN, asphaltene content and degree of biodegradation from Sørbø [76].

Crude Oil	Density [g/cm^3]	Viscosity [mPa·s]	TAN[76] [mgKOH/g]	Asphaltene[76] [wt%]	Biodegradation[76]
A	0.904 ± 0.005[70]	36 ± 2	3.01 ± 0.04	0.25*	Slight
B	0.934 ± 0.005	277 ± 14	2.0 ± 0.1	2.04 ± 0.05	Slight
C	0.891 ± 0.005	22 ± 1	0.98 ± 0.05	0.39 ± 0.01	Moderate

*Only one parallel, consequently no standard deviation.

From Table xx, it is clear that crude oil B has the highest density, viscosity and asphaltene content, followed by A and C respectively. Crude oil by B can be characterized as a heavy oil, using the API classification in section 2.2.1. Crude oil A and C can be characterized as medium oils, according to the API classification.

Crude oil A has the highest TAN, followed by B and C respectively. Crude oil C is the most biodegraded of the crudes, A and B are equally biodegraded.

4.2 Interfacial Tension

The IFT of decane in distilled water was measured to be 53.5 mN/m. The measurements were only run for 15 minutes, as the system seemed to come rapidly into equilibrium. The measured value for decane is close to the literature value by Goebel et al. [77], which is 53.2 mN/m.

4.2.1 Effect of Salinity

Results from measurements of IFT in brines with different NaCl concentrations, are shown in Figure 4.2.-4.4. IFT for all crude oils are displayed as a function of brine pH.

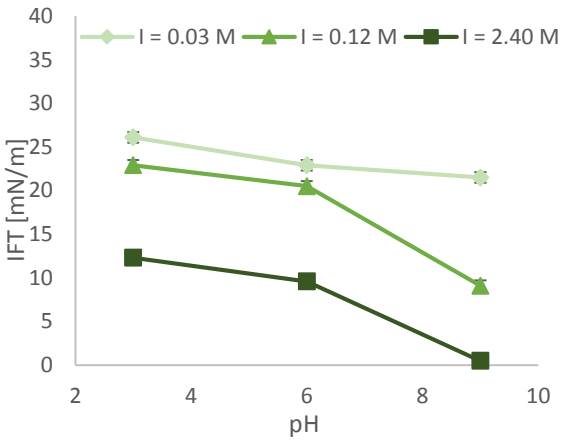

Figure 4.2. Measured IFT for crude oil A, as a function of pH. Measurements conducted at different NaCl concentrations.

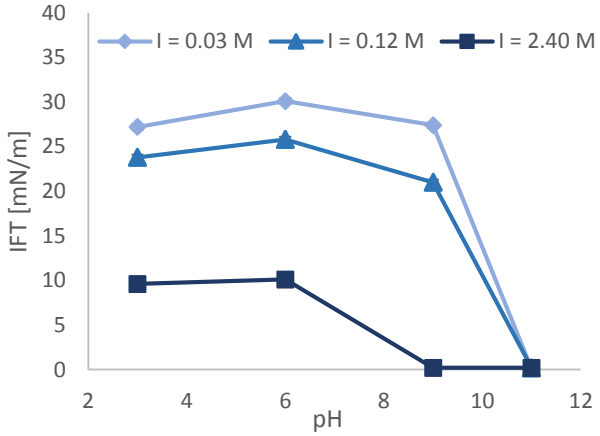

Figure 4.3. Measured IFT for crude oil B, as a function of pH. Measured at different NaCl concentrations.

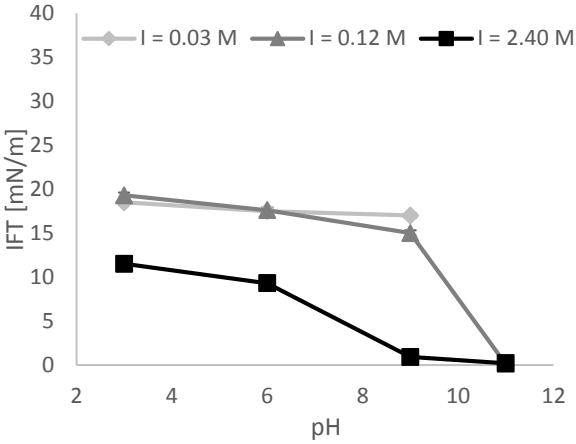

Figure 4.4. Measured IFT for crude oil C, as a function of pH. Measured at different NaCl concntrations.

The results in Figure 4.2-4.4 show that IFT decreases with increasing ionic strength at pH 3-9, as a main trend. The exception is crude oil C (Figure 4.4) at pH 3 and 6, where the measured IFT for the low and medium salinity brines are almost equal, but slightly higher for the medium salinity brine.

From Figure 4.2-4.4, it can be seen that the measured IFT for crude oil B is generally higher than the other crude oils. Crude oil C seem to have the lowest IFT values, and crude oil A seem to lie in between. The differences is more evident for the low and medium salinity brines, than for the high salinity brine.

The results also show that IFT decreases with increasing pH, as a main trend. Except for crude oil B, where the IFT increases from pH 3 to 6. At pH 11, IFT was not measureable for crude oil A in any of the investigated brines. IFT for crude oil C was not measureable in the low salinity brine at pH 11.

4.2.2 Presence of Ca^{2+} ions

Results from measurements of IFT in 0.03 M brines, with and without Ca^{2+} ions, are shown in Figure 4.5-4.7. IFT for all crude oils are displayed as a function of brine pH.

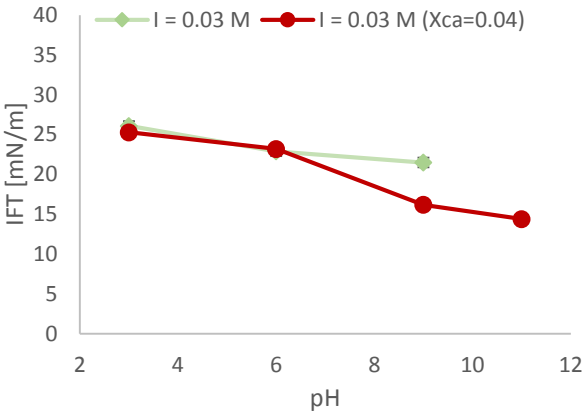

Figure 4.5. Measured IFT for crude oil A, as a function of pH. Measurements conducted at 0.03 M concentrations, with and without Ca^{2+} ions.

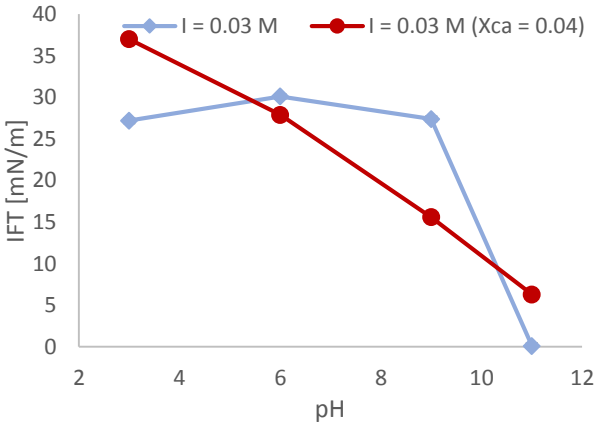

Figure 4.6. Measured IFT for crude oil B, as a function of pH. Measurements conducted at 0.03 M concentrations, with and without Ca^{2+} ions.

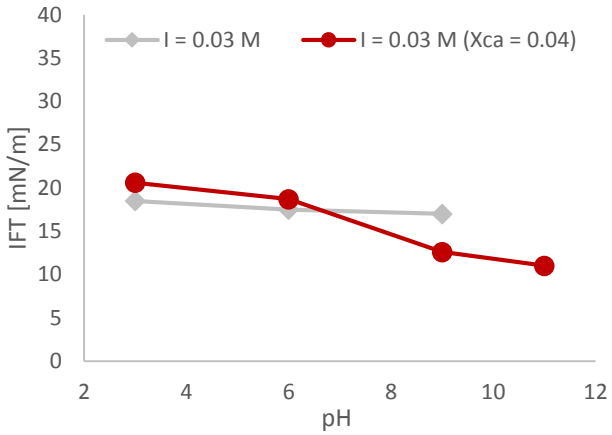

Figure 4.7. Measured IFT for crude oil C, as a function of pH. Measurements conducted at 0.03 M concentrations, with and without Ca^{2+} ions.

The results in Figure 4.5-4.7 show that IFT decreases with increasing pH for all crude oils in the calcium brines. At pH 11, the presence of Ca^{2+} ions increases the IFT for all crude oils noticeably compared to only monovalent ions. At pH 9, the presence of Ca^{2+} ions appear to reduce the IFT for all crude oils relative to brines with only monovalent ions. At low and neutral pH, the presence of Ca^{2+} ions does not appear to affect the results particularly, possibly except for crude oil B at low pH.

4.3 Zeta Potential

4.3.1 Variation of salinity

The measured zeta potential for crude oil A, B and C are presented in Figure 4.8-4.10, as a function of brine pH. A trend line has been drawn for the different samples, to illustrate the main features from the measurement results.

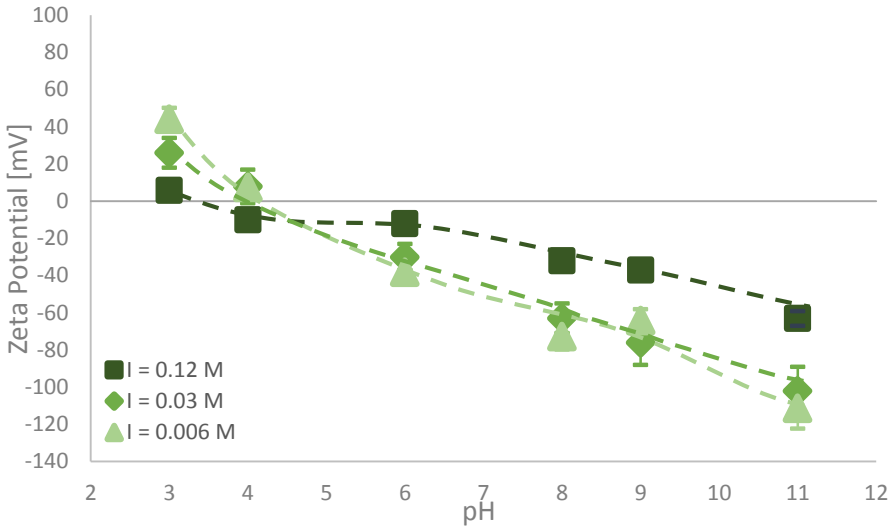

Figure 4.8. Measured zeta potential of crude oil A, as a function of pH.

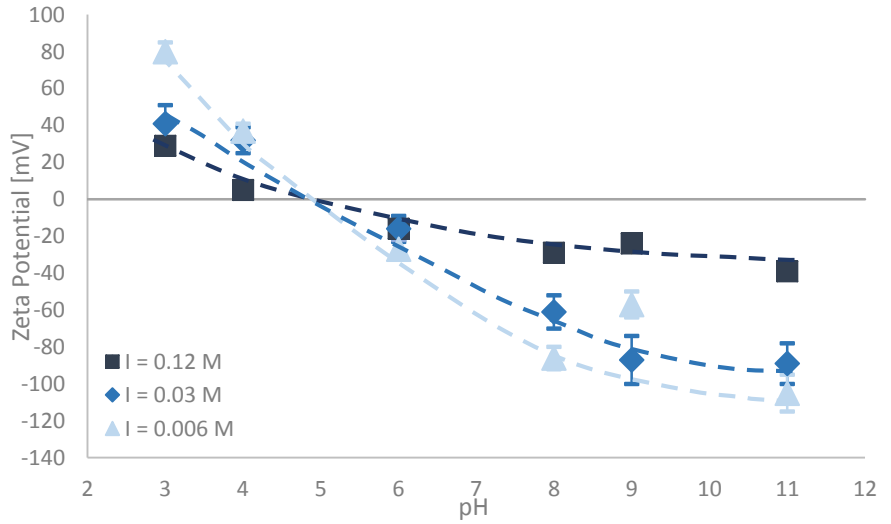

Figure 4.9. Measured zeta potential of crude oil B, as a function of pH.

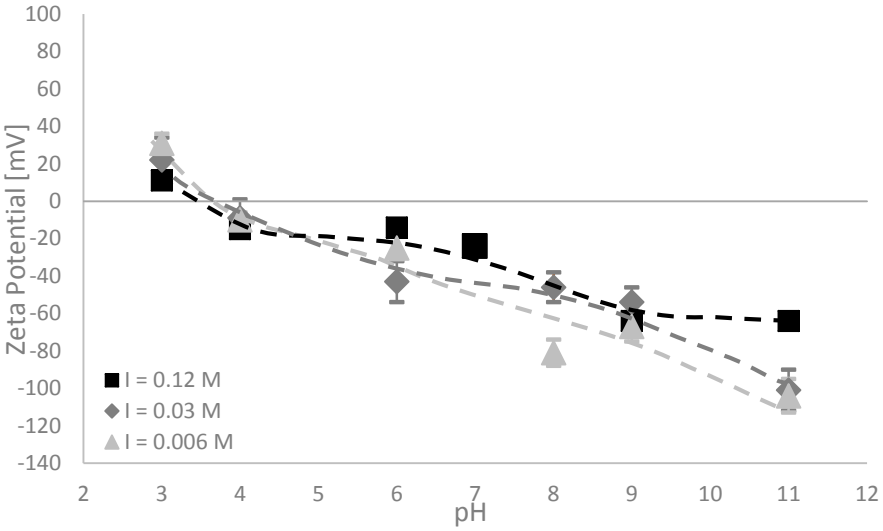

Figure 4.10. Measured zeta potential for crude oil C, as a function of pH.

The results represented in Figure 4.8-4.10, clearly indicates a dependency between zeta potential and pH, where the zeta potential decreases with increasing pH. The results also displays a clear indication of dependency of brine salinity, where the magnitude of the zeta potential decreases with increasing salinity. A shift from positive to negative zeta potential below neutral pH can be observed for all crude oils in Figure 4.8-4.10.

4.3.2 Effect of Ca^{2+} ions

The zeta potential of crude oil droplets in two 0.03 M brines have been measured, where one contains only monovalent Na^{+} cations and the other also have a small amount of divalent Ca^{2+} cations. The measured zeta potential for the three crude oils are presented in Figure 4.11-4.13 as a function of brine pH, which is varied from 3 to 11. A trend line has been drawn for the different samples, to illustrate the main features from the measurement results.

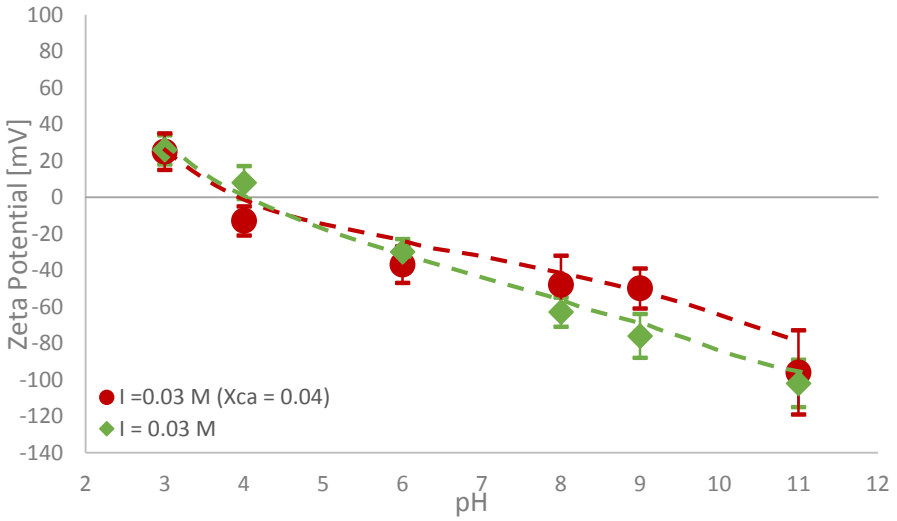

Figure 4.11. Measured zeta potential for crude oil A, as a function of pH.

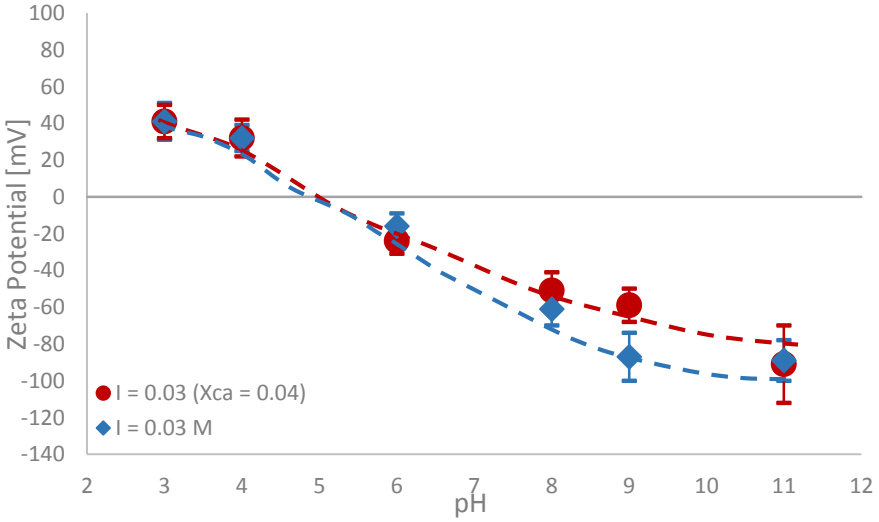

Figure 4.12. Measured zeta potential for crude oil B, as a function of pH.

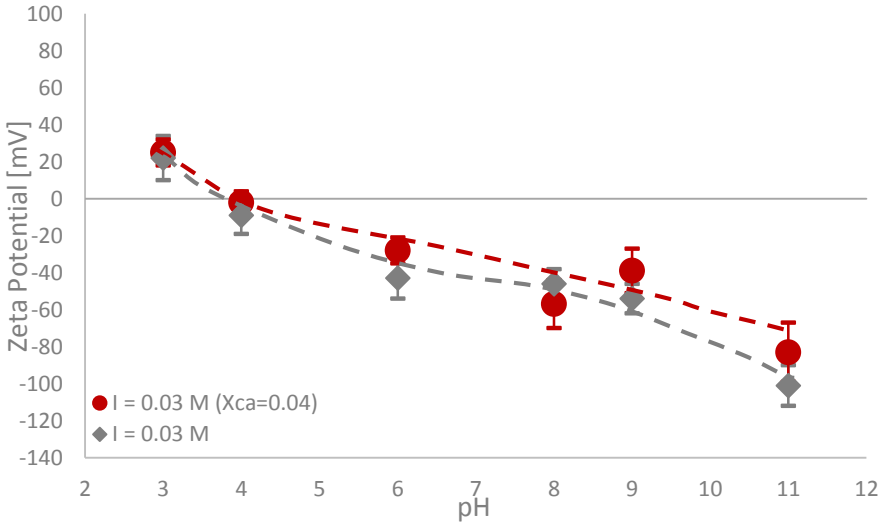

Figure 4.13. Measured zeta potential for crude oil C, as a function of

The results presented in Figure 4.11-4.13, also clearly indicate a dependency between zeta potential and pH, where the zeta potential decreases with increasing pH. It can be observed that the presence of calcium ions seem to reduce the magnitude of the measured zeta potential, particularly for the negative zeta potentials.

4.4 Contact Angle Measurements

The measured contact angles for crude oil A, B and C is shown in Figure 4.14-4.16, as a function of brine pH. The contact angles have been measured in 0.12 M and 2.40 M NaCl brines and 0.03 M brine with presence of calcium ions.

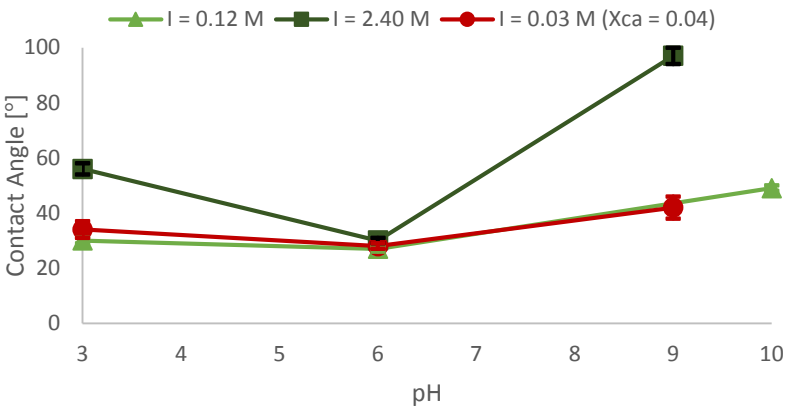

Figure 4.14. Contact angle versus brine pH, for crude oil A.

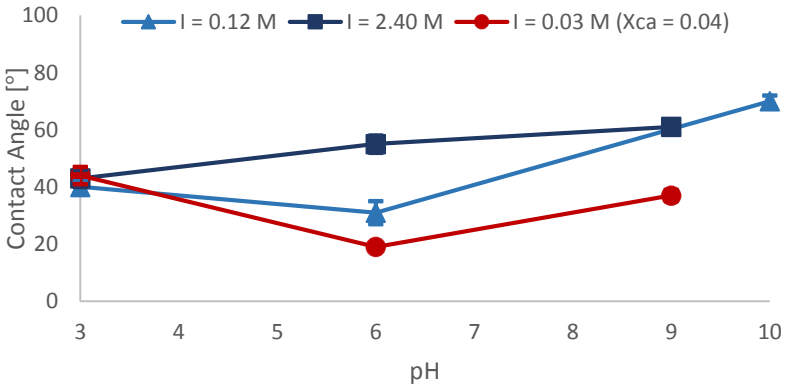

Figure 4.15. Contact angle versus brine pH, for crude oil B.

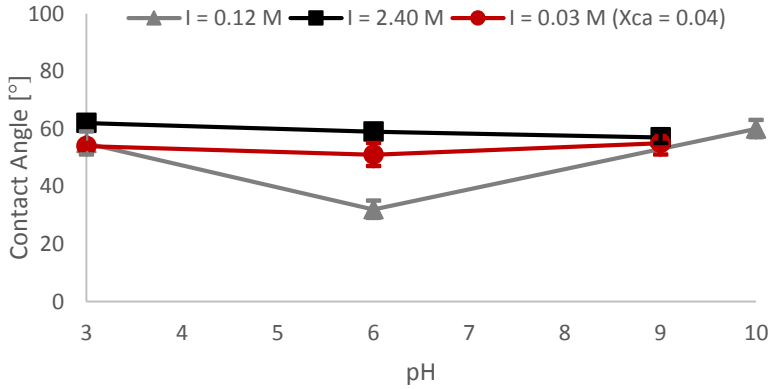

Figure 4.16. Contact angle versus brine pH, for crude oil C.

The results show that the contact angles appear to decrease from low to neutral brine pH, and increase from neutral to high pH in most cases. Exceptions from this trend can be observed for crude oil B (Figure 4.15) and C (Figure 4.16) in the high salinity brines. The contact angle for crude oil B increases from low to neutral pH, and the contact angle for crude oil C decreases from neutral to high pH.

5 Discussion

5.1 Interfacial Tension

The IFT for crude oils A and C decreases with increasing pH at any given salinity, see Figure 5.1 and 5.2. This can be explained by an increase in the dissociation of acids when the pH is increased [6, 19, 31-32, 47-48]. This behaviour might also indicate that crude oil A and C does not contain significant amounts of basic species, as these usually lower the IFT at low pH [33, 36, 43]. The IFT for crude oil A and C decreases with increasing salinity, except for crude oil C in the medium salinity brine.

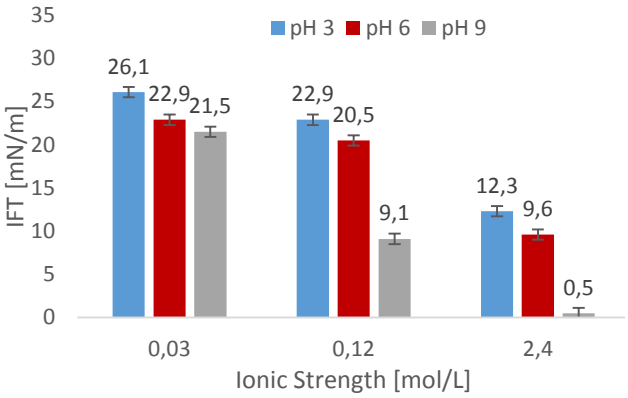

Figure 5.1. Displays the relationship between IFT and pH at different ionic strength for crude oil A.

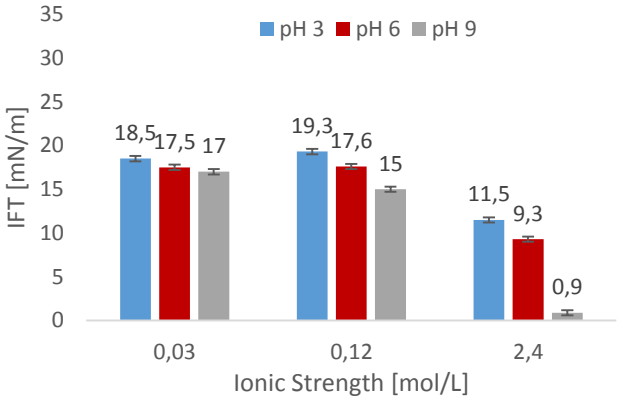

Figure 5.2. Displays the relationship between IFT and pH at different ionic strength for crude oil C.

Crude oil B, on the other hand, has its highest IFT value at pH 6 (Figure 5.3). This indicates a higher degree of basic functionality for crude oil B [33], but TBN has not been measured in this project so it is not possible to say for sure. Basic species in the crude oil are protonated at low pH, and this interfacial activity decreases the IFT.

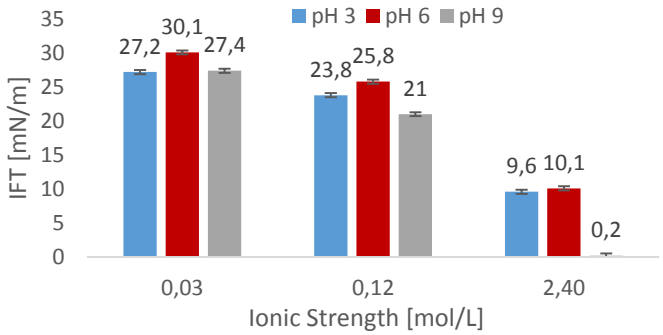

Figure 5.3. Displays the relationship between IFT and pH at different ionic strength for crude oil B.

From Figure 5.3, it is also clear that IFT decreases with increasing salinity for crude oil B.

At neutral pH, crude oil B has the highest IFT, followed by A and C respectively, regardless of brine salinity. This is illustrated in Figure 5.4:

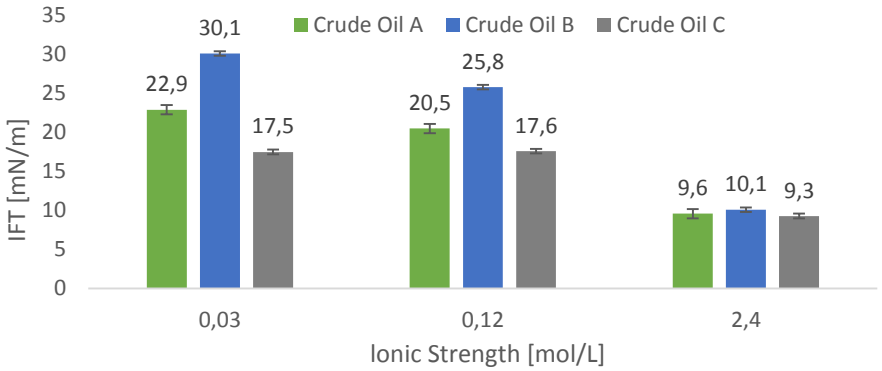

Figure 5.4. Measured IFT for crude oil A, B and C at neutral pH (pH 6), as a function of ionic strength.

The difference in IFT between the crude oils is particularly visible at low and medium salinity. The difference is smaller in the high salinity brine, probably due to the reduction of repulsion that further enhances surface activity [17]. From this, it is clear that crude oil C has the highest interfacial activity at neutral pH, even though Sørbø [76] found that it had the lowest TAN. This may be somewhat unexpected, as higher TAN values is often correlated with higher interfacial activity [31, 33]. Nevertheless, the low IFT values for crude oil C indicates that there are interfacial activity from acidic species. This further indicates that the acidic species present in crude oil C has a higher tendency for interfacial activity than the acidic species in the other crude oils. It is thus reasonable to suspect that interfacial activity depends on the structure of the acid-bearing molecules [31-32, 34]. Work by Varadaraj et al.[32] and Acevedo et al. [34] suggests that naphthenic acids of low molecular weight has a higher tendency for aggregating at the COB interface, thus promoting interfacial activity. Varadaraj et al. [32] further reported that primary naphthenic acids appeared to be more surface-active than secondary and primary naphthenic acids. This could suggest that the naphthenic acids in crude oil C are of lower molecular weight and/or have fewer substituents connected with the acid functional groups, than crude oil A and B.

Generally, the measured IFT of crude oil B is higher than for the other crudes. Sørbø [76] found that crude oil B has the highest asphaltene content of the three crude oils. This is consistent with findings from Buckley et al. [33], who reported that IFT is positively correlated with asphaltene content. Varadaraj et al. [31, 32] also suggested that asphaltene was not as effective in reducing

IFT as naphthenic acids, and that aggregation of asphaltenes at the COB interface probably decreases interfacial activity compared to naphthenic acids.

Crude oil A has the highest TAN, which could indicate that A should have the lowest IFT [31, 33]. However, the lowest IFT was observed for crude oil C, as discussed. This indicates that the acidic species in crude oil A have higher molecular weight and/or more substituents for the acid functional groups. The measured viscosity is somewhat higher for crude oil A than C. Buckley et al. [33] suggested that a dependency between TAN and viscosity indicates that acidic species in the crude oil associate, and thus can exert influence on viscosity rather than on IFT. This could indicate that the acidic species in crude oil A associate in the bulk of the crude oil, forming large complexes that increases the viscosity and at the same time prevents the acidic functional groups from aggregating at the COB interface.

The most notable effect in IFT can be observed at pH 11 for all crude oils in absence of calcium ions, in Figure 4.2-4.4. All crude oils showed either very low IFT or was not measureable by the pendant drop method at this pH. Such effects at high pH has been reported numerous times in literature, by for instance Buckley et al. [33], among others. This indicates that there are high degree of interfacial activity at high pH, presumably a high degree of dissociation of the naphthenic acids [6, 19, 31-33]. The results at pH 11 further indicates that all crude oils tend to form stable emulsions at these conditions [31-32]. No mentionable difference can be observed for the crude oils at pH 11.

At neutral pH, the presence of calcium ion appear to increase the IFT for crude oil C, but decrease IFT for crude oil B. There is a slight increase for crude oil A, but within the error margins. These effects are shown in Figure 5.5:

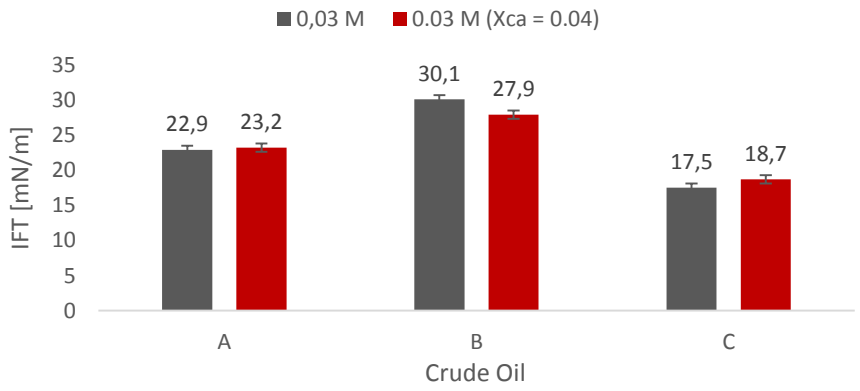

Figure 5.5. Effect of calcium ions at neutral brine pH, with 0.03 M ionic strength. Presence of calcium ions (Xca = 0.04) in red bars, and absence of calcium ions in black bars.

The increase in IFT with presence of calcium ions for crude oil C (and possibly A) could be explained by the calcium ions' ability to form complexes with the dissociated naphthenic acids [36]. Tichelkamp et al. [36] explained that a 1:2 ion pair of calcium and dissociated naphthenic acids show less interfacial activity and higher oil solubility, and can thus migrate to the oil phase. This increase in IFT with calcium ions present in the brine is most evident at pH 11, for all crude oils (see Table 5.1). As discussed earlier, crude oil C shows the lowest IFT values, which indicates that there are more interfacial activity. This is probably the reason for why crude oil C experiences the largest effect of calcium ions at neutral pH.

The presence of calcium ions at pH 11 increases the IFT notably for all crude oils (Table 5.1), where the IFT was unmeasureable or slightly above zero in the absence of calcium ions.

Table 5.1. IFT for crude oils A, B and C at brine pH 11 in the presence of calcium ions.

Crude Oil	**A**	**B**	**C**
IFT [mN/m]	14.4 ± 0.6	6.3 ± 0.3	11.0 ± 0.3

The increase in IFT at pH 11 is greatest for crude oil A, followed by C and B respectively. The relative effects of calcium ions are probably larger at high pH because a significant number of the acid groups are expected to be dissociated here [36-37]. The effect of calcium ions appear to be lowest for crude oil B, which could indicate that crude oil B has the lowest concentration of acidic functional groups at the interface. Crude oil B has the highest asphaltene content. An aggregation of the asphaltenes at the interface was suggested not to promote interfacial activity to the same extent as naphthenic acids, by Varadaraj et al. [31-32]. This may indicate that there a less acidic functionality at the interface for crude oil B.

It is worth mentioning that the complete opposite trend is observed at pH 9, with brines containing calcium ions. At pH 9, the IFT decreases in presence of calcium ions, for all crude oils. This does not seem to be explainable by the formation of ion pairs, as discussed for pH 11.

5.2 Zeta Potential

As mentioned, Figure 4.8-4.10 clearly indicates a dependency between zeta potential and pH, where the zeta potential decreases with increasing pH. This trend is consistent with existing literature [40, 43-45], and arises from the dissociation of naphthenic acids above the IEP. The dissociation of the naphthenic acids yields a more negative surface, and thereby a more negative zeta potential. A dependency of brine salinity has also been observed, in Figure 4.8-4-10. High salinity brines gives the lowest (negative or positive) zeta potentials, and the zeta potentials further increases with decreasing salinity. This correlates well with existing literature, where increasing ion concentration decreases the Debye length. A decrease in Debye length implicates less electrophoretic mobility, and consequently a decreasing zeta potential [17, 33, 43].

Comparing the zeta potential for the three crude oils in 0.03 M NaCl brine, shows that the trends are quite similar for the crudes, see Figure 5.6:

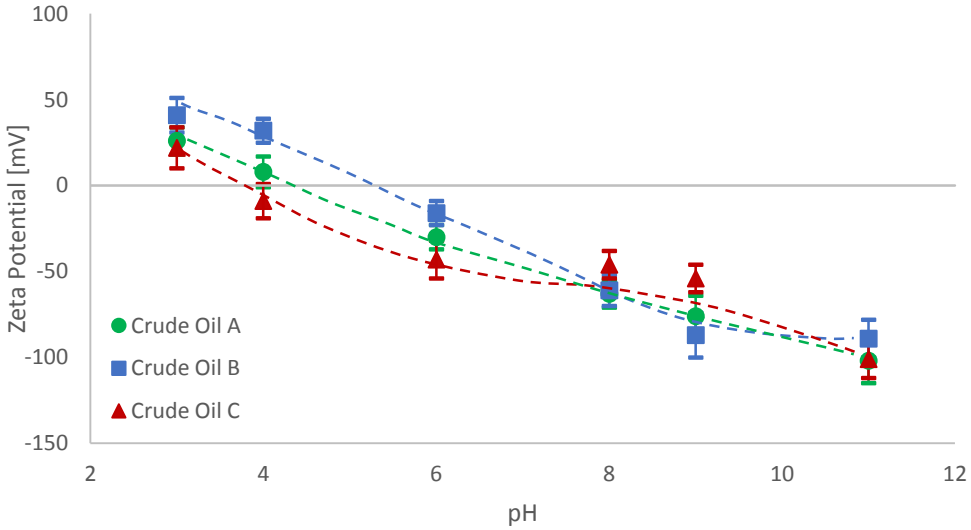

Figure 5.6. Measured zeta potential in 0.03 M brine for crude oil A, B and C, as a function of brine pH.

The most notable differences between the crudes can be observed at pH 3–6. At pH 3-4, particularly at pH 4, B has the highest positive zeta potential followed by A and C respectively. At pH 6, B has the smallest negative zeta potential, also followed by A and C respectively. Above this pH, the differences between the crudes become less pronounced and there does not seem to be a consistent trend. The difference between the crude oils is most notable at low pH also in the lowest salinity brine (0.006 M), in Figure 5.7. The crude oils follow the zeta potential order of B>A>C at pH 3-4, but above this pH the measured zeta potentials seem to coincide.

A possible explanation for why no profound differences can be observed between the crude oils at high pH in the low salinity brines, is that adsorption of hydroxide ions can contribute to the negative zeta potential [51]. More variation can be observed in the highest salinity brine (0.12 M), in Figure 5.8:

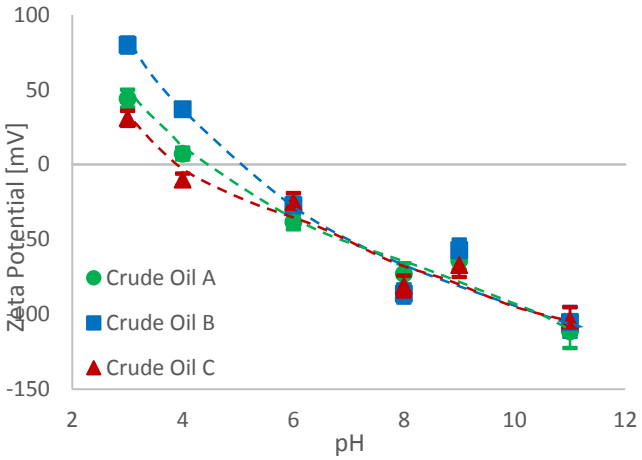

Figure 5.7. Measured zeta potential in 0.006 M brine for crude oil A, B and C, as a function of brine pH.

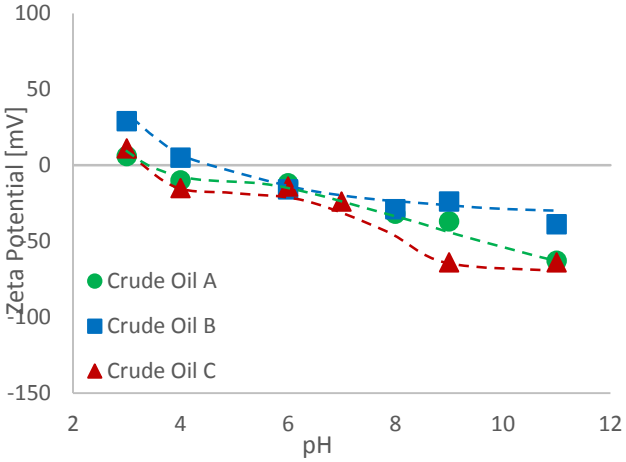

Figure 5.8. Measured zeta potential in 0.12 M brine for crude oil A, B and C, as a function of brine pH.

Crude oil B clearly has the highest zeta potential at low pH, also in the highest salinity brine, but the differences between A and C is less clear. At high pH, the measured zeta potential is notably less negative for B than for A and C. However, it should be stressed that it was not possible to obtain values for standard deviation at this salinity, which possibly could lead to more overlap. Nevertheless, from IFT measurements it was indicated that crude oil C had the highest degree of interfacial activity and crude oil B had the lowest degree of interfacial activity. This could be what is observed in Figure 5.8. If more acidic species are present at the interface of crude oil C, a higher degree of acid dissociation are likely to take place, than for crude oil B. This again leads to a more negative charge. However, this effect is not observed for the brines of lower salinity. In the high salinity brine, the electric charge from the double layer is considerably weaker than for lower salinities [17]. This may possibly result in a more "crude oil-character" in the measured zeta potential.

The fact that crude oil B has the highest zeta potentials at low pH, regardless of salinity, may indicate a higher TBN/TAN ratio than for the other crudes. This is because basic species are protonated at low pH [43, 47, 49, 51], thus yielding a more positive zeta potential. Barth et al. [21] found a strong correlation between TBN and asphaltene content. Considering that crude

oil B has the highest asphaltene content, this could further indicate that B also has the highest TBN.

For all three crude oils, there is a shift from negative to positive zeta potential, meaning that there exists an IEP [17]. At which pH the different crude oils appear to have their IEP based on the trends in Figure 4.8-4.10, is tabulated in Table 5.2.

Table 5.2. Displays at which pH the crude oils have their IEP. Values are estimated from Figure 4.8-4.10.

Crude Oil	A	B	C
IEP [pH]	4	5	3.5

The existence of an IEP indicates presence of both acidic and basic interfacial-active components at the COB interface [43, 49, 51]. It is clear that the IEP for crude oil B lies at a higher pH than for the other crude oils. The IEP tends to increase with increasing TBN/TAN ratio, due to protonation of basic species at low pH [43, 49]. As discussed above, crude oil B has the highest asphaltene content and thus, possibly more species of a basic nature than A and C. The IEP appear to be at a slightly lower pH for crude oil C than crude oil A, even though crude oil A has a considerably higher TAN. This could indicate that crude oil A has a slightly higher TBN/TAN ratio than crude oil C [43, 49], even though crude oil C has a slightly higher asphaltene content. This could arise from crude oil C being the most biodegraded, and not necessarily having a high nitrogen content as basic oil species often have [31-32]. However, IFT measurements indicates that the acidic crude oil components is more interfacially active in crude oil C than A, which could also be an explanation for the zeta potential results.

Crude oil A has the highest TAN, which could indicate that it contains acidic species of various structures and different pK_a values. These acids may dissociate at different pH values, and could maybe explain why the zeta potential for crude oil A shows a decrease with increasing pH in all regions. Crude oil B (in 0.12 M and 0.03 M brine) and C (in 0.12 M brine), on the other hand, have small regions where no further decrease can be observed in zeta potential with increasing pH. This could indicate that all acid functional groups have dissociated at this point for A and C.

The measured zeta potential for crude oil A, B and C in 0.03 M brine at pH 3-8, is shown in Table 5.3:

Table 5.3. Displays the measured zeta potential for crude oil A, B and C in 0.03 M brine at pH 3-8, in order to compare with emulsion stability at zeta potential larger than ±30 mV.

Crude Oil	pH 3	pH 4	pH 6	pH 8
A	26 ± 8	8 ± 9	-30 ± 7	-63 ± 8
B	41 ± 10	32 ± 7	-16 ± 7	-61 ± 9
C	22 ± 12	-9 ± 10	-43 ± 11	-46 ± 8

Assuming that emulsions are stable if the magnitude of the zeta potential is larger than ±30 mV [71], the emulsion stability of the different crude oils in 0.03 M brine can be assessed by evaluating the zeta potentials in Table 5.3. At pH 8, and above, all crude oils appear to form stable emulsions. At pH 6, crude oil B does not appear to form stable emulsion, as opposed to crude oil A and C. At the lower pH region, crude oil B appear to form stable emulsions, but not A and C. It should, however, be stressed that the standard deviations are relatively large, so it is difficult to decide the emulsion stability with great certainty. The fact that crude oil B only seem to form unstable emulsions at neutral pH can possibly correlate with the observed peak at this pH in IFT measurements (Figure 4.3), as high IFT is an indication of low emulsion stability.

By comparing the zeta potential of the 0.03 M salinities in Figure 4.11-4.13, it is clear that the presence of calcium ions lowers the magnitude of the zeta potential, as expected [51-52]. The effect of calcium ions is particularly visible at negative zeta potential. Because the calcium ions are divalent, they offer a more efficient screening of the negative particle surface compared to monovalent ions. Calcium ions can also form positively charged complexes [51] or ion-pairs with dissociated naphthenic acids in the crude oil [36], which would reduce the negative charge.

The standard deviation calculated in the software seems to increase with increasing pH (see Appendix III for exact values). In particular, the standard deviations at pH 11 are high. It was hypothesised that the increasing deviation could arise from increasing temperature from the ultrasonic bath, but this was ruled out as following measurements were conducted with samples in random order and the trend for the standard deviation remained the same. The standard deviations for the calcium brines are generally higher than for the other brines at equivalent pH. This implies that there is a greater uncertainty connected with zeta potential measurements at high pH, and with divalent ions. The uncertainties at high pH could possibly come from a more vigorous dissociation of the naphthenic acids, making the activity at the interface higher and consequently more difficult measure exact. The higher uncertainties connected with divalent ions could possibly arise from the Ca^{2+} ions ability to form complexes with crude oil

components [36, 51]. The calcium ions form complexes with dissociated acids, if the complex formation is ongoing during measurements it may lead to variations in the measured potentials.

A positive zeta potential for the COB system implicates that there will be attraction with a negatively charged silica surface (assuming pzc around pH 2 [43]), thus promoting oil-wetting. A negative zeta potential for the COB system indicates that there will repulsion with the negatively charged silica surface, thus promoting water-wetness. [17, 43, 47-48] Based on measurements of zeta potential for the crude oils, one could expect attraction between the crude oils and silica at low pH, and repulsion at high pH. Increased water-wetness can, in some cases, contribute to improved oil recovery [8].

5.3 Contact Angle

The contact angle increases when going from neutral to high pH for almost every measurement series. This does not coincide with what one would expect. An increase in pH is expected to increase the negative charge at the COB interface due to dissociation of naphthenic acids. This would in turn lead to more repulsion between the COB and solid/brine interfaces, and consequently decrease the contact angles. The reason for these measured contact angles could be the change in drop profile during measurements at high pH, screenshots of a drop over time is shown in Figure 5.9.

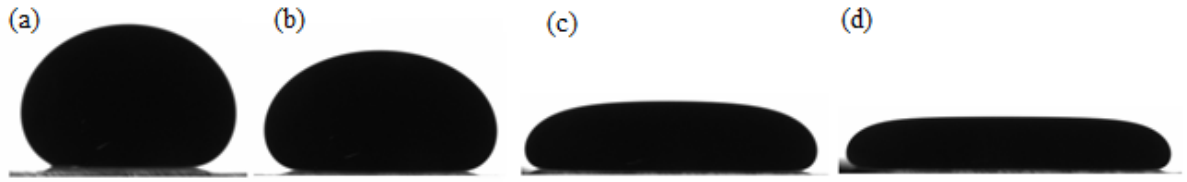

Figure 5.9. Changes in drop profile during contact angle measurements for crude oil A in 0.12 M NaCl brine, at pH 10. Drop profile after (a) 1 minute, (b) 3 minutes, (c) 5 minutes and (d) 7 minutes.

As seen in Figure 5.9, the drop smears out on the glass plate after some time. To some degree, this happened for all crude oils at high pH in the NaCl brines. If the drop was close to the edge of the glass plate, it eventually slid off the plate with no visible oil residues left on the glass plates. Measurements of the contact angle from the drop profile in Figure 5.9(d), does not seem to provide good results. The fact that the droplets tended to slid off the plates during measurements indicates that there is no attraction between the oil and solid phase. The conclusion for the measurements of contact angles at high pH is that even though the measured contact angles are not very small, there is large repulsion between the glass and oil phase and the glass plate is strongly water-wet. A possible reason for the behaviour in Figure 5.9 is that the drop volumes (7 µL) were too large and consequently affected by the gravitational force. A drop volume of 1 µL was tested for crude oil C, but still showed a tendency to spread. It seems reasonable to assume that the solid surface is in fact strongly water-wet at high pH for all crude oils, and that the measured contact angles are not representative for the observed effects.

Presence of calcium cations may increase the contact angle between crude oil droplets and the solid surface at elevated pH. This is because of the possible bridging between the solid/brine and COB interfaces [3, 36, 54, 56]. At high pH more acids will have dissociated, leading to a more negative surface charge making the bridging effect more evident. The values for the measured contact angles in the calcium brines are given in Table 5.4.

Table 5.4. Measured contact angles in calcium brines, at different pH.

Crude Oil	pH 3	pH 6	pH 9
A	34 ± 3	28 ± 1	42 ± 4
B	44 ± 3	19 ± 1	37 ± 2
C	54 ± 1	51 ± 4	55 ± 4

From Table 5.4 (and Figure 4.11-4.13), the contact angle clearly increases when the pH is increased from a neutral to a high value. However, this increase could also be a result from the effect discussed for Figure 5.9.

Comparing the contact angles in Table 5.4 and 5.5, shows that the calcium brine and the 0.12 M brine produces almost identical contact angles at low pH. At neutral pH, the calcium brine produces somewhat higher contact angles (except for crude oil B). Since the ionic strength of the brines are not equal, it is difficult to accurately compare the results. Nevertheless, the presence of calcium ions appear to increase the contact angles significantly, especially considering that the ionic strength is lower.

Table 5.5. Measured contact angles in 0.12 M and 2.40 M NaCl brines, at pH 3 and 6.

Crude Oil	0.12 M		2.40 M	
	pH 3	pH 6	pH 3	pH 6
A	30 ± 1	27 ± 1	56 ± 2	30 ± 1
B	40 ± 2	31 ± 4	34 ± 3	55 ± 3
C	55 ± 4	32 ± 3	62 ± 1	59 ± 1

The high-salinity brine, in most cases, produce the highest contact angles. This can be explained by compression of the electrical double layers, which in turn causes a less stable water film and consequently a less water-wet surface [17]. Such a destabilization of the water film makes it easier for the polar molecules in the crude oil to interact with the silica surface [57]. This is consistent with findings from, among others, Nasrella et al [52] who found that low salinity brines resulted in more water-wet surfaces. However, when the brine salinity is very high, such as 2.40 M, the electrical double layer will be compressed to such an extent that it is practically non-existing (see section 3.1.2). This means that electrostatic interactions does not contribute significantly to interactions between the phases. In cases of such high salinities, the crude oil may stick onto the solid surface [52].

The decrease in contact angle when increasing the pH from low to neutral, could be explained by the presence of any basic spices in the crude oil. At low pH, the basic functional groups are protonated, yielding a positively charged COB interface that will be attracted to the negatively charged solid/brine interface. At neutral pH, both crude oil and silica will have a slight negative charge and will thus experience repulsion [40, 51-52]. This decrease can be observed for all crude oils (see Table 5.4-5.5, and Figure 4.14-4.16). One exception is observed for crude oil B in high-salinity brine, which show an increase from low to neutral pH. Measurements of zeta potential of crude oil B at neutral pH showed a negative charge, which indicates that a repulsion between the COB and solid/brine interfaces should occur. The increase in contact angle from low to neutral pH can possibly be explained by the very high salinity, as previously discussed. A high salinity may possibly enable the oil to stick to the solid surface, as the effects of electrostatics does not contribute significantly. However, it seems peculiar that this increase can only be observed for one of the crude oils. Consequently, explaining this behaviour proves difficult and more investigation is necessary.

Crude oil C appears to have the largest contact angles regardless of pH and ionic strength. Crude oil C has the lowest density, and thus the highest API gravity. Buckley et al. [57] reported that crude oils with increasing API gravity appeared to be poorer solvents for their asphaltenes, and consequently there is an increased possibility for precipitation of asphaltene on the solid surface. Crude oil C was also observed to have the lowest IFT values, indicating a high degree of interfacial activity by acidic functional groups. Such groups are likely to be attracted to a silica surface, thus making it less water-wet [57]. This is consistent with the observed contact angle measurements.

For crude oil B at low pH, all contact angles are approximately identical in the different brines. This trend can also be observed for crude oil A at pH 6. Thus, it appears that compression and/or expansion of the electrical double layers does not occur in these cases, or that the effect is insignificant relative to other mechanisms. Such mechanisms could be that the oil sticks to the solid phase due to high salinity [52], as discussed earlier. However, this seems unlikely, as this effect is not observed at other pH values.

At these short time scales, and in the presence of brine, neither of the investigated conditions seem to lead to significant interactions between the crude oil and the silica surface.

5.4 Correlation of the Investigated Properties

Table 5.6 provides a comparison of the investigated crude oil properties. The various properties have been simplified to a scale from 'highest-to-lowest', where 1 is highest and 3 is lowest.

Table 5.6. Comparison of measured properties for the crude oil in low-salinity brines on a scale of 1 – 3, where 1 is the highest value and 3 is the lowest value.

Crude oil	A	B	C
Density	2	1	3
Viscosity	2	1	3
TAN	1	2	3
Asphaltene content	3	1	2
IFT at pH 3-9	2	1	3
pH at IEP	2	1	3
|Zeta potential at low pH (0.03 M)|	2	1	3
|Zeta potential at neutral pH (0.03 M)|	2	3	1

From the Table, crude oil B often tend to have the 'highest' values, crude oil C the 'lowest' and crude oil A is in between. The following grossly simplified correlations can be made:

- Crude oil A has intermediate density, viscosity, asphaltene content, IFT and IEP. However, crude oil A has the highest TAN.
- Crude oil B has the highest density, viscosity, asphaltene content, IFT, IEP and zeta potential at low pH. Crude oil B also have an intermediate TAN and the least negative zeta potential at neutral pH.
- Crude oil C has the lowest density, viscosity, TAN, IFT, IEP and zeta potential at low pH. However, crude oil C have the highest contact angles.

6 Conclusion

The objective of this thesis has been to investigate the physiochemical properties of three different crude oils, and correlate these properties with the crude oil composition. This has been carried out by investigating the IFT and zeta potential in the COB system, and contact angles for the COBR system. The brine phase has been varied with regards to pH, salinity and cation type. Density and viscosity of the crude oils have also been investigated in this thesis. Crude oil properties with regards to TAN, asphaltene content and degree of biodegradation has been provided by Sørbø [G]. Crude oil A was found to have the highest TAN and lowest asphaltene content. Crude oil B was found to have the highest density, viscosity and asphaltene content. Crude oil C was found to have the lowest density, viscosity and TAN, and the most biodegraded.

From the IFT results, it was observed that the IFT decreased with increasing pH, for all crude oils. It was hypothesized that this was because of an increase in dissociation of naphthenic acids with increasing pH, thus leading to more surface activity. This trend was also observed for the zeta potential measurements; the zeta potential decreased with increasing pH. The zeta potential trends were also hypothesized to arise from the dissociation of naphthenic acids, as this would suggest a more negative surface charge.

Both IFT and zeta potential decreased with increasing salinity at a given pH, for all crude oils. The decrease in IFT was hypothesized to arise from a reduction in electrostatic repulsion, thus increasing the interfacial concentration of dissociated acids. The reduction in zeta potential was suggested to come from a decrease in the electrical double layer, which would decrease the electrophoretic mobility and thus lower the zeta potential.

The most drastic effects in the IFT measurements were observed at high pH for all crude oils. At high pH, the IFT was either not measureable by the pendant drop method, or slightly above zero. It was found that presence of small amounts of Ca^{2+} ions increased the IFT considerably at pH 11. It was suggested that this was because of formation of a complex of calcium ions and dissociated naphthenic acids, facilitating a migration to the oil phase. However, the presence of Ca^{2+} ions was found to lower the IFT notably at pH 9. The presence of calcium ions also tended to lower the magnitude of negative zeta potentials at neutral and high pH.

Crude oil C proved to have the highest degree of interfacial activity at low, neutral and high pH. This was unexpected, as crude oil C had the lowest TAN. However, it was hypothesized that the acidic component may be of lower molecular weight and perhaps a primary structure,

which may favour aggregation at the interface. Crude oil C also appeared to have to highest contact angles at low pH, implicating a less water-wet behaviour than the other crude oils. High contact angles is consistent with high interfacial activity, as the polar compounds in the crude oil may be attracted to the solid surface. It was also hypothesized that crude oil C may experience asphaltene precipitation in contact with a solid phase. Crude oil C had the lowest zeta potentials at low pH, and the lowest IEP, indicating a low TBN/TAN ratio compared to the other crude oils.

Crude oil B showed the lowest interfacial activity, which appeared to be correlated with the high asphaltene content. Crude oil B was also observed to have the highest zeta potential at low pH, and the highest IEP, indicating a high TBN/TAN ratio compared to the other crude oils. Crude oil B showed an increase in IFT from low to neutral pH, which is an indication of basic functionality in the crude oil. The TBN for the crude oils has not been measured, but the physiochemical investigations indicates a presence of basic species.

Even though crude oil A had the highest TAN, it did not show the highest degree of interfacial activity. It was hypothesized that interactions between the acidic components in the bulk prevented the acidic molecules from being active at the interface, and thus exerting influence on the crude oil viscosity.

It proved difficult to observe any clear trends in the contact angle results. However, it did seem like crude oil C had the overall highest contact angles. At high pH it was observed that the crude oil droplets tended to slid of the glass plates. It was hypothesized that this was an effect of a strongly water-wet solid surface, even though the measured contact angles did not reflect this.

7 Further Work

Multivariate analysis

A multivariate analysis could prove useful to identify correlations between crude oil composition and physical-chemical properties. In order to observe trends it would also be useful to increase the number of investigated crude oils. More investigation into the crude oil composition would also be useful for correlation with physical-chemical properties. Particularly TBN, and investigations of the structures of both naphthenic acids and asphaltenes, with emphasis on polar functional groups.

TBN

There have been indications that one of the investigated crude oils have a significantly higher TBN/TAN than the other crude oils. It could thus be interesting to investigate whether this is the case, or if it could have been other effects.

Emulsion stability

There have been indications that the investigated crude oils may form stable emulsions at elevated pH. This is based on IFT and zeta potential measurements. Zeta potential measurements indicated that one of the crude oils may not form stable emulsions at neutral pH, in contrast to the other two crude oils. Further investigation into the crude oils ability form stable emulsions would thus be interesting.

Contact Angles and Wettability

Rock mineralogy plays a major importance in waterflooding. It is thus important to investigate the crude oils effect on wettability on reservoir rocks. A suggestion is to improve the method utilized in this thesis. Another washing procedure was suggested in this thesis. It could also be useful to study wettability with emphasis on drop profile and drop volume, as the drop profile was observed to change during measurements. Measurements conducted with glass plates aged in brine or crude oil could also prove useful for correlation with waterflooding effects.

8 References

[1] Sheng, J. (2011). *Modern Chemical Enhanced Oil Recovery: Theory and Practice*. Burlington: Gulf Professional Publishing.

[2] Terry, R.E. (2001). Enhanced Oil Recovery. In: *Encyclopaedia of Physical Science and Technology*, 3rd ed. San Diego: Academic Press, pp. 503-518.

[3] Farooq, U.; Asif, N.; Tweheyo, M.T.; Sjöblom, J.; Øye, G. (2011). Effect of Low-Saline Aqueous Solutions and pH on the Desorption of Crude Oil Fractions from Silica Surfaces. *Energy Fuels*. **25**(5), pp. 2058-2064.

[4] Johannessen, A.M.; Spildo, K. (2014). Can Lowering the Injection Brine Salinity Further Increase Oil Recovery by Surfactant Injection under Otherwise Similar Conditions?. *Energy Fuels*. **28**(11), pp. 6723-6734.

[5] Hamon, G. (2016). Low-Salinity Waterflooding: Facts, Inconsistencies and the Way Forward. *Petrophysics*. **57**(1), pp. 41-50.

[6] Alotabi, M.B.; Nasr-El-Din, H.A. (2009). Effect of Brine Salinity on Reservoir Fluids Interfacial Tension. *SPE EUROPEC/EAGE Annual Conference and Exhibition*. Amsterdam, The Netherlands: June 8-11, 2009

[7] Schobert, H.H. (2013). *Chemistry of Fossil Fuels and Biofuels*. Cambridge: Cambridge University Press.

[8] Borgun, A.E. (2007). *Crude oil components with affinity for gas hydrates in petroleum production*. PhD. University of Bergen.

[9] Shi, Q.; Hou, D.; Xu, C.; Zhao, S.; Zhang, Y. (2010). Characterization of Heteroatom Compounds in a Crude Oil and Its Saturates, Aromatics, Resins, and Asphaltenes (SARA) and Non-basic Nitrogen Fractions Analyzed by Negative-Ion Electrospray Ionization Fourier Transform Ion Cyclotron Resonance Mass Spectrometry. *Energy Fuels*. **24**(4), pp. 2545-2553.

[10] Sjöblom, J.; Aske, N.; Auflem, I.H.; Brandal, Ø.; Havre, T.E.; Sæther, Ø.; Westvik, A.; Johnsen, E.E.; Kallevik, H. (2003). Our current understanding of water-in-crude oil emulsions.: Recent characterization techniques and high pressure performance. *Advances in Colloid an Interface Science*. **100-102**(1), pp. 399-473.

[11] De Ghetto, G.; Paone, F.; Villa, M. (1995). Pressure-Volume-Temperature for Heavy and Extra Heavy Oils. *SPE International Heavy Oil Symposium*. Calgary: Canada, 19-21 June.

[12] Kidnay, A.J.; Parrish, W.R.; McCartney, D.G. (2011). *Fundamentals of Natural Gas Processing*. 2nd ed. Boca Raton: CRC Press.

[13] Ciarlet, P.G.; Glowinski, R.; Xu, J. (2011). *Handbook of Numerical Analysis. Volume 16: Numerical Methods for Non-Newtonian Fluids.* Oxford: North-Holland.

[14] March, N.H.; Tosi, M.P. (2002). Introduction to Liquid State Physics. Singapore: World Scientific.

[15] Hutin, A.; Argillier, J.-F.; Langevin, D. (2014). Mass Transfer between Crude Oil and Water. Part 1: Effect of Oil Components. *Energy Fuels*. **28**(12), pp. 7331-7336.

[16] Cpieng.com, (2014). Lab Services: Total Acid Number. [online] Available at: http://www.cpieng.com/totalAcidNumber.htm [Accessed 24.05.2016].

[17] Berg, J. C. (2010). *An Introduction to interfaces & colloids: The Bridge to Nanoscience.* Singapore: World Scientific Publishing Co. Pte. Ltd.

[18] Buckley, J.S. (1994). *Chemistry of the Crude Oil/Brine Interface*. Proceedings of the 3rd International Symposium on Evaluation of Reservoir Wettability and Its Effect on Oil Recovery. Laramie. pp. 33-38.

[19] Poteau, S.; Argillier, J.-F. (2005). Influence of pH on Stability and Dynamic Properties of Asphaltenes and Other Amphiphilic Molecules at the Oil-Water Interface. *Energy & Fuels*. **19**(4), pp. 1337-1341.

[20] Sjöblom, J.; Aske, N.; Auflem, I.H.; Brandal, Ø.; Havre, T.E.; Sæther, Ø.; Westvik, A.; Johnsen, E.E.; Kallevik, H. (2002). Our current understanding of water-in-crude oil emulsions. Recent characterization techniques and high pressure performance. *Advances in Colloid and Interface Science*. **100-102**(1), pp. 399-473.

[21] Barth, T.; Høiland, S.; Fotland, P.; Askvik, K.M.; Myklebust, R.; Erstad, K. (2005). Relationship between the Content of Asphaltenes and Bases in Some Crude Oils. *Energy Fuels*. **19**(4), pp. 1624-1630.

[22] Zolotukhin, A.B.; Ursin, J.R. (2000). *Introduction to Petroleum Reservoir Engineering*. Kristiansand: Høyskoleforlaget: Norwegian Academic Press.

[23] Farooq, U.; Asif, N.; Tweheyo, M.; Sjöblom, J.; Øye, G. (2011). Surface Characterization of Model, Outcrop, and Reservoir Samples in Low Salinity Aqueous Solutions. *Journal of Dispersion Science and Technology*. **32**(4), pp. 519-531.

[24] Kulkarni, R.D.; Somasundaran, P. Effect of Pretreatments on the Electrokinetic Properties of Quartz. (1977). *International Journal of Mineral Processing*. **4**(2), pp. 89-98.

[25] Prasanphan, S.; Nuntiya, A. (2006). Electrokinetic Properties of Kaolins, Sodium Feldspar and Quartz. *Chiang Mai J. Sci*. **33**(2), pp. 183-190.

[26] Berry, J. D.; Neeson, M. J.; Dagastine, R. R.; Chan, D. Y. C.; Tabor, R.F. (2015). Measurement of surface and interfacial tension using pendant drop tensiometry. *Journal of Colloid and Interface Science*. **454**, pp. 226-237.

[27] Langevin, D.; Poteau, S.; Hénaut, I; Argillier, J.F. (2004). Crude Oil Emulsion Properties and their Applications to Heavy Oil Transportation. *Oil & Gas Science and Technology*. **59**(5), pp. 511-521.

[28] Buckley, J.S.; Fan, T. (2005). Crude Oil/Brine Interfacial Tensions. *International Symposium of the Society of Core Analysts*. Toronto, Canada: August 21-25, 2005.

[29] Kelesoglu, S.; Meakin, P.; Sjöblom, J. (2011). Effect of Aqueous Phase pH on the Dynamic Interfacial Tension of Acdic Crude Oils and Myristic Acid in Dodecane. *Journal of Dispersion Science and Technology*. **32**(11), pp. 1682-1691.

[30] Rubin, E.; Radke, C.J. (1979). Dynamic Interfacial Tension Minima in Finite Systems. *Chemical Engineering Science*. **35**(5), pp. 1129-1138.

[31] Varadaraj, R.; Brons, C. (2007). Molecular Origin of Heavy Oil Interfacial Activity Part 1: Fundamental Interfacial Properties of Asphaltenes Derived from Heavy Crude Oils and Their Correlation To Chemical Composition. *Energy & Fuels*. **21**(1), pp. 195-198.

[32] Varadaraj, R.; Brons, C. (2007). Molecular Origins of Heavy Crude Oil Interfacial Activity Part 2: Fundamental Interfacial Properties of Model Naphthenic Acids and Naphthenic Acids Separated from Heavy Crude Oils. *Energy & Fuels*. **21**(1), pp. 199-204.

[33] Buckley, J.S; Fan, T. Crude Oil/Brine Interfacial Tensions. *Petrophysics*. **48**(3), pp. 175-185.

[34] Acevedo, S.; Escobar, G.; Ranaudo, M.A.; Khazen, J.; Borges, B.; Pereira, J.C.; Mendez, B. (1998). Isolation and Characterization of Low and High Molecular Weight Acidic Compounds from Cerro Negro Extraheavy Crude Oil. Role of These Acids in the Interfacial Properties of the Crude Oil Emulsions. *Energy Fuels*. **13**(2), pp. 333-335.

[35] McMurry, J. (2011). *Fundamentals of Organic Chemistry*. 7th edition. Belmont: Brooks/Cole, Cengage Learning.

[36] Tichelkamp, T.; Teigen, E.;Nourani, M.; Øye, G. (2015). Systematic study of the effect of electrolyte composition on interfacial tensions between surfactant solutions and crude oils. *Chemical Engineering Science*. **132**(1), pp. 244-249.

[37] Havre, T.E.; Sjöblom, J.; Vindsatd, J.E. (2003). Oil/Water-partitioning and interfacial behaviour of naphthenic acids. *Journal of Dispersion Science Technology*. **24**(6), pp. 789-801.

[38] Hunter, R. J. (1981). *Zeta Potential in Colloid Science: Principles and Applications*. San Diego: Academic Press.

[39] Shukla, A.; Rehage, H. (2008). Zeta Potentials and Debye Screening Lengths of Aqueous, Viscoelastic Surfactant Solutions (Cetyltrimethylammonium Bromide/Sodium Salicylate System). *Langmuir*, **24**(16), pp. 8507-8513.

[40] Hirasaki, G.J. (1991). Wettability: Fundamentals and Surface Forces. *Society of Petroleum Engineers*. **6**(2), pp. 217-226.

[41] Lyklema, J.; Rovillard, S.; De Coninck, J. (1998). Electrokinetics: The Properties of the Stagnant Layer Unraveled. *Langmuir, The ACS Journal of Surfaces and Colloids*. **14**(20), pp. 5659-5663.

[42] Malvern Instruments Ltd. (2007). Zetasizer Nano User Manual, MANO317. 3rd ed. England.

[43] Buckley, J.S.; Takamura, K.; Morrow, N.R. (1989). Influence of Electrical Surface Charges on the Wetting Properties of Crude Oils. *SPE Reservoir Engineering*. **4**(3), pp. 332-340.

[44] Buckley, J.S.; Takamura, K.; Morrow, N.R. (1989). Influence of Electrical Surface Charges on the Wetting Properties of Crude Oils. *SPE Reservoir Engineering*. **4**(3), pp. 332-340.

[45] Schwuger, M.J.; Stockdorn, K. (1995). Microemulsions in Technical Processes. *Chem. Rev*. **95**(4), pp. 849-864.

[46] Nasralla, R.A.; Bataweel, M.A; Nasr-El-Din, H.A. (2013). Investigation of Wettability Alteration and Oil-Recovery Improvement by Low-Salinity Water in Sandstone Rock. *Journal of Canadian Petroleum Technology*. **52**(2), pp. 144-154.

[47] Parra-Barraza, H.; Hernández-Monitel, D.; Lizardi, J.; Hernández, J.; Urbina, R.H.; Valdez, M.A. (2002). The zeta potential and surface properties of asphaltenes obtained with different crude oil/*n*-heptane proportions. *Fuel*. **82**(8), pp. 869-874.

[48] Sadeqi-Moqadam, M.; Riahi, S.; Bahramian, A. (2016). An investigation into the electrical behaviour of oil/water/reservoir rock interfaces: The implication for improvement in wettability prediction. *Colloids and Surfaces A: Physiochemical and Engineering Aspects*. **490**(1), pp. 268-282.

[49] Dubey, S.T.; Doe, P.H. (1993). Base Number and Wetting Properties of Crude Oils. *SPE Reservoir Engineering*. **8**(3), pp. 195-200.

[50] Liu, X.; Yan, W.; Stenby, E.H.; Thormann, E. (2016). Release of Crude Oil from Silica and Calcium Carbonate Surfaces: On the Alternation of Surface and Molecular Forces by High- and Low-Salinity Aqueous Salt Solutions. *Energy Fuels*. (Submitted manuscript DOI: 10.1021/acs.energyfuels.6b00569)

[51] Farooq, U.; Simon, S.; Tweheyo, M.T.; Sjöblom, J.; Øye, G. (2013). Electrophoretic Measurements of Crude Oil Fractions Dispersed in Aqueous Solutions of Different Ionic Compositions — Evaluation of the Interfacial Charging Mechanisms. *Journal of Dispersion Science and Technology*. **34**(10), pp. 1376-1381.

[52] Nasralla, R.A; Nasr-El-Din, H.A. (2014). Impact of cation type and concentration in injected brine on oil recovery in sandstone reservoirs. *Journal of Petroleum Science and Engineering*. **122**(1), pp- 384-395.

[53] Yang, J.; Dong, Z.; Dong, M.; Yang, Z.; Lin, M.; Zhang, J.; Chen, C. (2016). Wettability Alteration during Low-Salinity Waterflooding and the Relevance of Divalent Ions in This Process. *Energy Fuels*. **30**(1), pp. 72-79.

[54] Abdallah, W.; Buckley, J.S.; Carnegie, A.; Edwards, J.; Herold, B.; Fordham, E.; Graue, A.; Habashy, T.; Seleznev, N.; Signer, C. et al. (2007). Fundamentals of Wettability. *Oilfield Review*. **19**(2), pp. 44-61.

[55] Craig Jr., F.F. (1971). *The Reservoir Engineering Aspects of Waterflooding*. Dallas: SPE of AIME.

[56] Yang, J.; Dong, Z.; Yang, Z.; Lin, M. (2015), Wettability Alteration by Salinity and Calcium Bride in a Crude Oil/Brine/Rock System. *Petroleum Science and Technology*. **33**(19), pp. 1660-1665.

[57] Buckely, J.S.; Liu, Y.; Monsterleet, S. (1998). Mechanisms of Wetting Alteration by Crude Oils. *SPE Journal*. **3**(1), pp. 54-61.

[58] Liu, Q.; Dong, M.; Yue, X.; Hou, J. (2005). Synergi of alkali and surfactant in emulsification of heavy oil in brine. *Colloids and Surfaces A: Physicochemical and Engineering Aspects*. **273**(1-3), pp. 219-228.

[59] Buckley, J.S.; Morrow, N. (2011). Improved Oil Recovery by Low-Salinity Waterflooding. *Journal of Petroleum Technology*. **63**(5), pp. 106-112.

[60] Hadia, N.J.; Hansen, T.; Tweheyo, M.T.; Torsæter, O. (2012). Influence of Crude Oil Components on Recovery by High and Low Salinity Waerflooding. *Energy Fuels*. **26**(7), pp. 4328-4335.

[61] Sandengen, K.; Tweheyo, M.T.; Raphaug, M.K.; Kjølhamar, A.; Crescente, C.; Kippe, V. (2011). Experimental Evidence of Low-Salinity Waterflooding Yeilding a More Oil-Wet Behaviour. *Paper presented at the International Symposium of the Society of Core Analysts.* Austin: USA. 18-21 September, 2011.

[62] McGuire, P.L.; Chatham, J.R.; Paskvan, F.K. Sommer, D.M.; Carini, F.H. (2005). Low Salinity Oil Recovery: An Exciting New EOR Opportunity for Alaska's North Slope. *SPE Proceedings of the Western Reginal Meeting*. Irvine: USA. March 30-April 1.

[63] Lager. A.; Webb, K.J.; Black, C.J.J.; Singleton, M.; Sorbie, K.S. (2008). Low Salinity Oil Recovery - An Experimental Investigation1. *Petrophysics*. **49**(1), pp. 28-35.

[64] RezaeiDoust, A.; Puntervold, T.; Strand, S.; Austad, T. (2009). Smart Water as Wettability Modifier in Carbonate and Sandstone: A Discussion of Similarities/Differences in the Chemical Mechanisms. *Energy Fuels*. **23**(9), pp. 4479-4485.

[65] Gandomkar, A.; Rahimpour, M.R. (2015). Investigation of Low-Salinity Waterflooding in Secondary and Tertiary Enhanced Oil Recovery in Limestone Reservoirs. *Energy Fuels*. **29**(), pp. 7781-7792.

[66] anton-paar.com. (2016). *Anton Paar GmbH, Glossary*. [Online] Retrieved at: http://www.anton-paar.com/corp-en/good-density-measurement/glossary/ [Accessed 18.04.2016]

[67] Picker, P.; Tremblay, E.; Jolicoeur, C. A High-Precision Digital Readout Flow Densimeter for Liquids. (1974). *Journal of Solution Chemistry*. 3(5), pp. 377-384.

[68] Atkins, P.; De Paula, J. (2010). *Physical Chemistry*. 9th ed. Oxford: Oxford University Press.

[69] Maier, G. DataPhysics Instruments GmbH. (2002). Operating Manual DataPhysics OCA, version 2.05. Filderstadt.

[70] Rønsberg, T. (2015). *An investigation of the correlation between interfacial properties and phase composition in the crude oil/water system*. MSc. University of Bergen.

[71] Malvern.com. (2014). *Zeta potential quality report for the Zetasizer Nano*. [online] Available at: http://www.malvern.com/en/support/resource-center/technical-notes/TN101104ZetaPotentialQualityReportZetasizerNano.aspx [Accessed 06.05.2016]

[72] Andresen, C. L. (2013). *Physical Chemistry of Mechanisms for Low Salinity Waterflood*. MSc. University of Bergen.

[73] Hogg, R. V.; Tanis, E. A. (2010). *Probability and Statistical Inference*. 8th edition. New Jersey: Pearson Prentice Hall.

[74] Malvern.com. (2016). [online] Available at: http://www.malvern.com/en/products/product-range/kinexus-range/kinexus-pro-plus/default.aspx [Accessed 26.05.2016]

[75] Biolinscientific.com. (2016). [online]. Available at: http://www.biolinscientific.com/zafepress.php?url=%2Fpdf%2FAttension%2FTheory%20Notes%2FAT-TN-06-Influence-drop-volume-contact-angle.pdf [Accessed 02.02.2016]

[76] Sørbø, G. (2016). *Polar Components in Crude Oils and their Correlations to Physiochemical Properties*. MSc. University of Bergen.

[77] Goebel, A.; Lunkenheimer, K. (1997). Interfacial Tension of the Water/*n*-Alkane Interface. *Langmuir*. **13**(2), pp. 369-372.

[78] Malvern.com. (2016). [online] Available at: http://www.malvern.com/en/products/product-range/kinexus-range/kinexus-pro-plus/default.aspx [Accessed 26.05.2016]

Appendix I: Calculations

This appendix contains all data used to calculate the results represented in this thesis.

Unless otherwise stated, standard deviation σ has been calculated based on the following equation:

$$\sigma = \sqrt{\frac{1}{n-1}\sum_{i=1}^{n}(x_i - \bar{x})^2} \qquad \textit{Equation A.1}$$

Where n is the number of parallels, x_i is the value of parallell i, and $\bar{x}$ is the average of the parallels. [analty]

Propagation of unceartainty has been calculated by the following equation:

$$e = \sqrt{\sum_{i=1}^{n} e_i} \qquad \textit{Equation A.2}$$

Where e_i is the error of measurements i. [analyt]

Appendix II: IFT Results

The IFT values that have been studied in this thesis is given in Table A-1. A-2 and A-3. The plot for each experimental run is given in Figure A1-A66.

Table A-1. Measured IFT for crude oil A. Standard deviation ±0.6 mN/m.

Brine (Ionic Strength [M])	Interfacial Tension [mN/m]			
	pH 3	pH 6	pH 9	pH 11
0.03 M	26.1	22.9	21.5	-
0.12 M	22.9	20.5	9.1	-
2.40 M	12.3	9.6	0.5	-
0.03 M (X_{Ca} = 0.04)	25.3	23.2	16.4	14.4

Table A-2. Measured IFT for crude oil B. Standard deviation ±0.3 mN/m.

Brine (Ionic Strength [M])	Interfacial Tension [mN/m]			
	pH 3	pH 6	pH 9	pH 11
0.03 M	30.1	27.2	27.4	0.1
0.12 M	23.8	25.8	21.0	0.2
2.40 M	9.6	10.1	0.2	0.2
0.03 M (X_{Ca} = 0.04)	37.0	27.9	15.6	6.3

Table A-3. Measured IFT for crude oil C. Standard deviation ±0.3 mN/m.

Brine (Ionic Strength [M])	Interfacial Tension [mN/m]			
	pH 3	pH 6	pH 9	pH 11
0.03 M	18.5	17.5	17.0	-
0.12 M	19.3	17.6	15.0	0.1
2.40 M	11.5	9.3	0.9	0.2
0.03 M (X_{Ca} = 0.04)	20.6	18.7	12.6	11.0

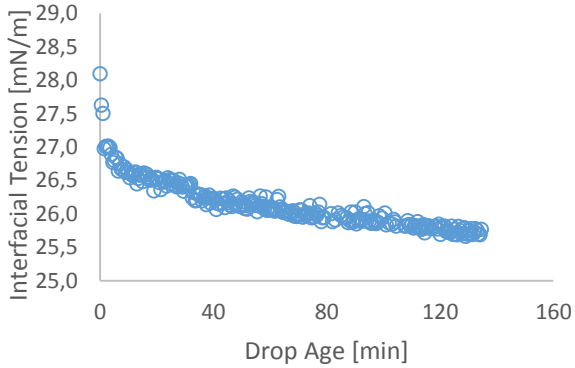

Figure A1. Crude oil A. Brine: 0.03 M NaCl,

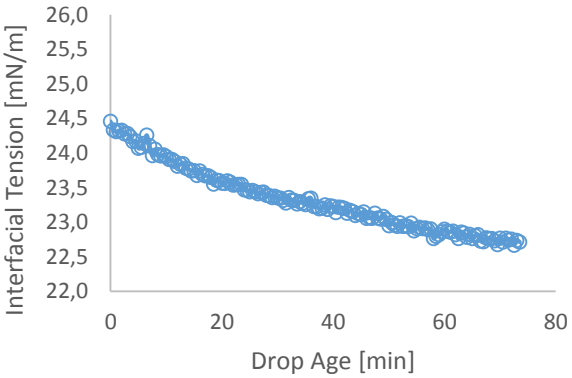

Figure A2. Crude oil A. Brine: 0.12 M, pH3.

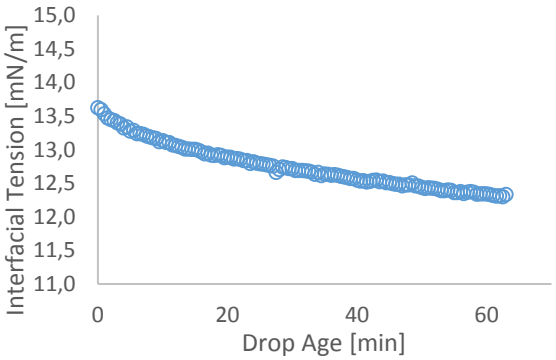

Figure A3. Crude oil A. Brine: 2.40 M, pH3.

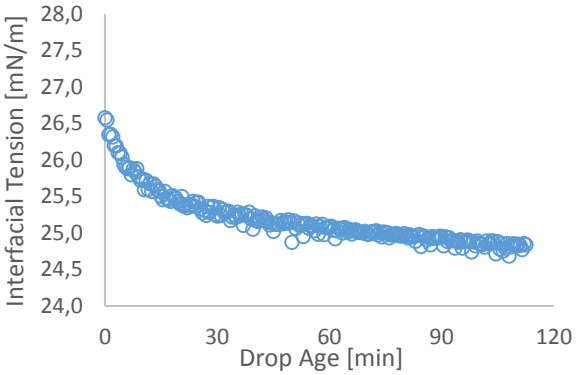

Figure A4. Crude oil A. Brine 0.03 M (Xca=0.04), pH3.

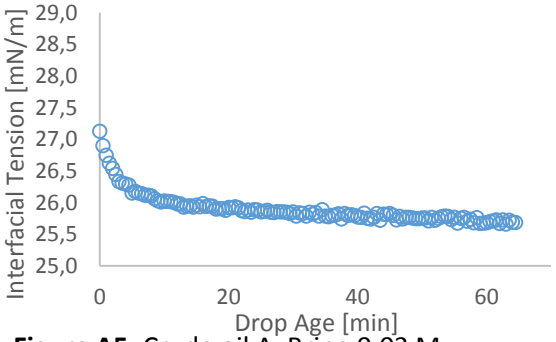

Figure A5. Crude oil A. Brine 0.03 M (Xca=0.04), pH3.

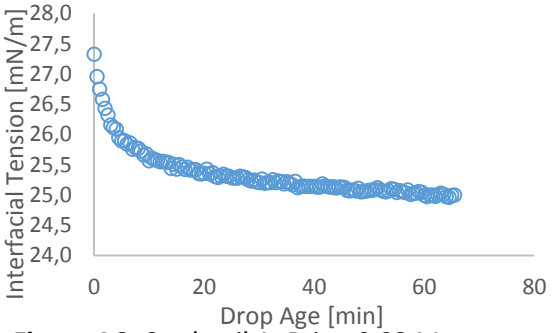

Figure A6. Crude oil A. Brine 0.03 M (Xca=0.04), pH3.

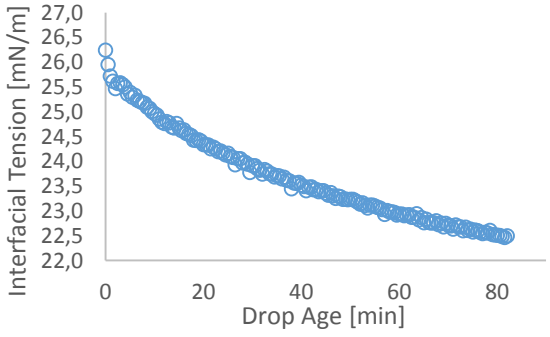

Figure A7. Crude oil A. Brine: 0.03M, pH6.

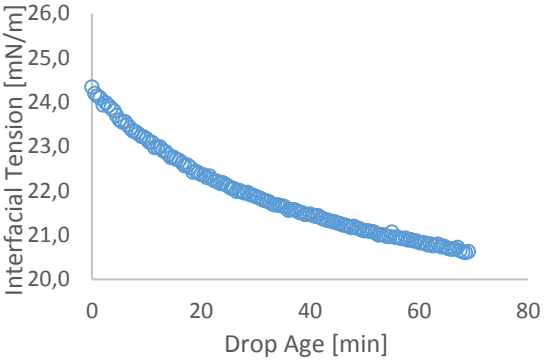

Figure A8. Crude oil A. Brine: 0.12 M, pH 6.

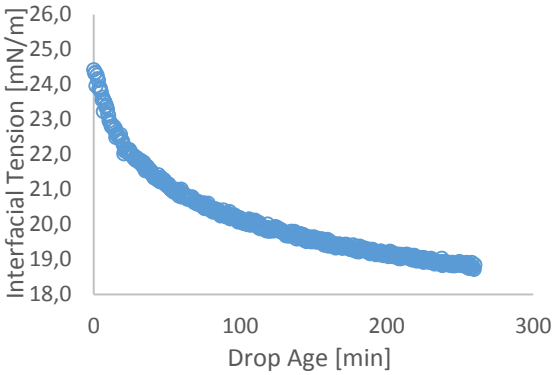

Figure A9. Crude oil A. Brine: 0.12 M, pH 6.

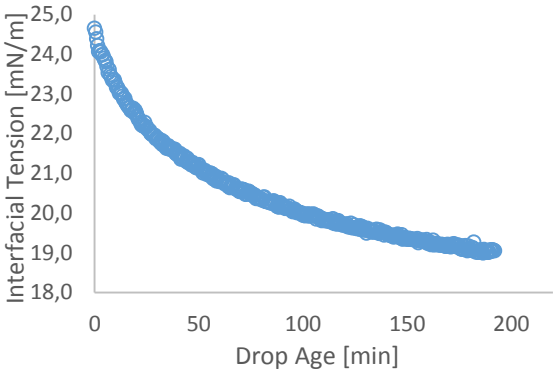

Figure A10. Crude oil A. Brine: 0.12 M, pH 6.

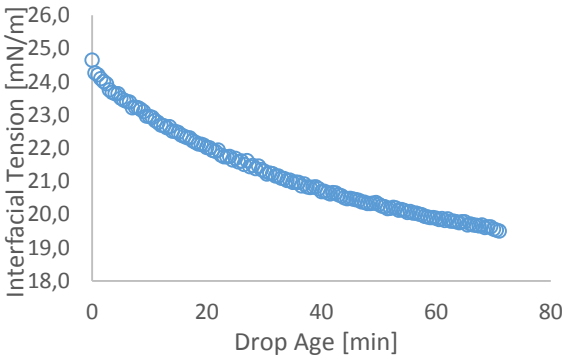

Figure A11. Crude oil A. Brine: 0.12 M, pH 6.

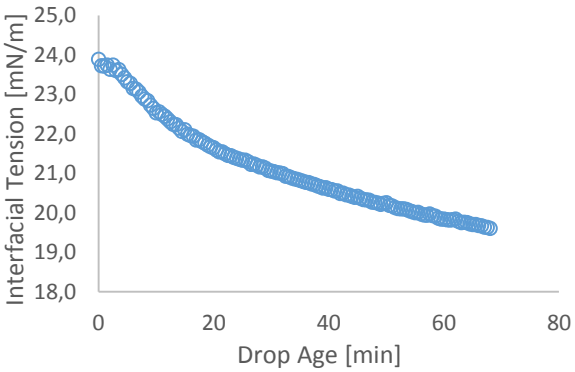

Figure A12. Crude oil A. Brine: 0.12 M, pH 6.

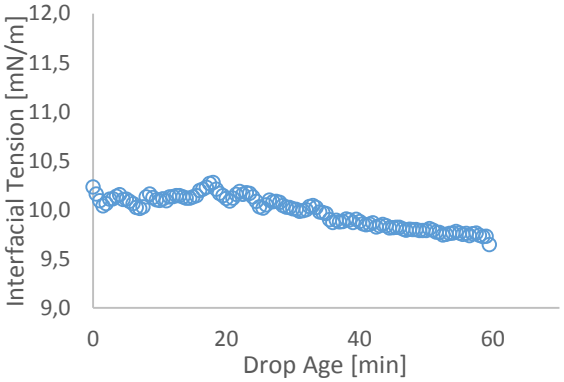

Figure A13. Crude oil A. Brine: 2.40 M, pH 6.

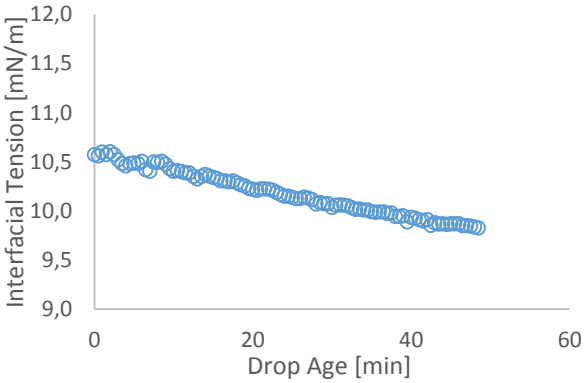

Figure A14. Crude oil A. Brine: 2.40 M, pH 6.

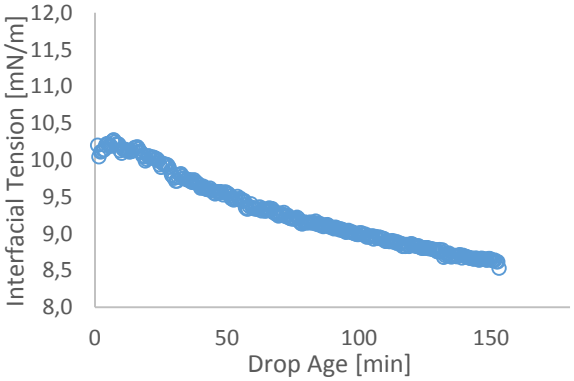

Figure A15. Crude oil A. Brine: 2.40 M, pH 6.

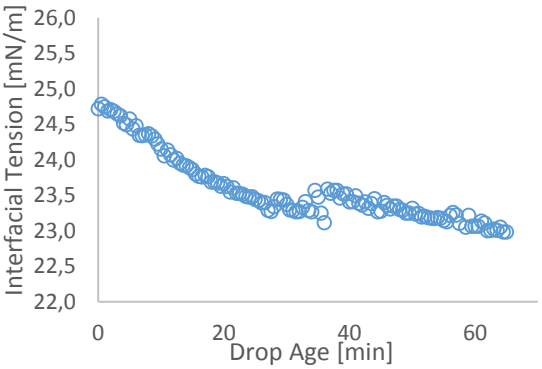

Figure A16. Crude oil A. Brine: 0.03 M (Xca=0.04), pH6.

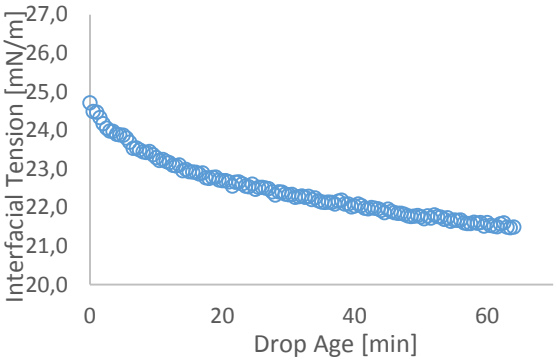

Figure A17. Crude oil A. Brine: 0.03 M, pH 9.

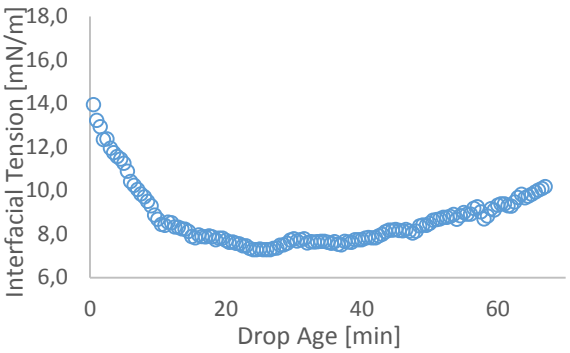

Figure A18. Crude oil A. Brine: 0.12 M, pH 9.

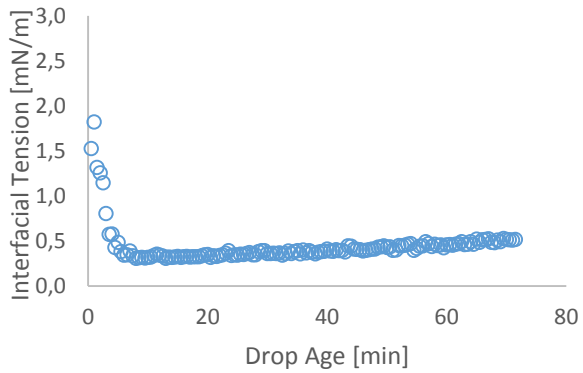

Figure A19. Crude oil A. Brine: 2.40 M, pH 9.

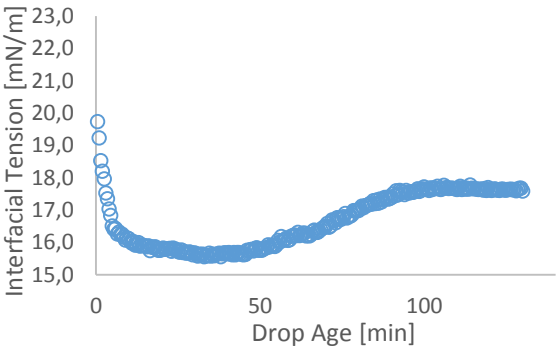

Figure A20. Crude oil A. Brine: 0.03 M (Xca=0.04), pH 9.

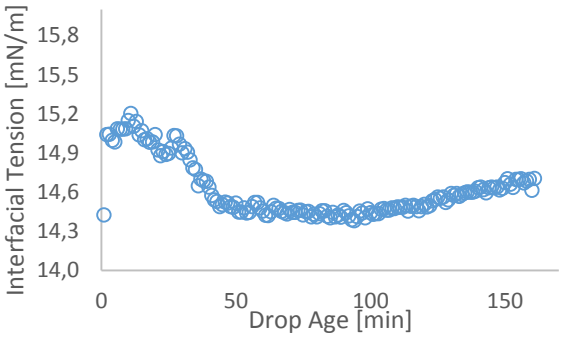

Figure A21. Crude oil A. Brine: 0.03 M (Xca=0.04), pH 11.

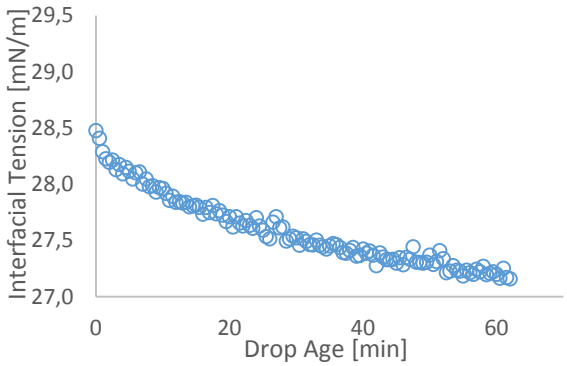

Figure A22. Crude oil B. Brine: 0.03M, pH 3.

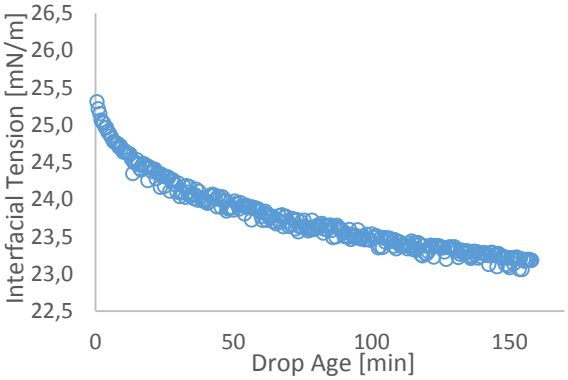

Figure A23. Crude oil B. Brine: 0.12 M, pH 3.

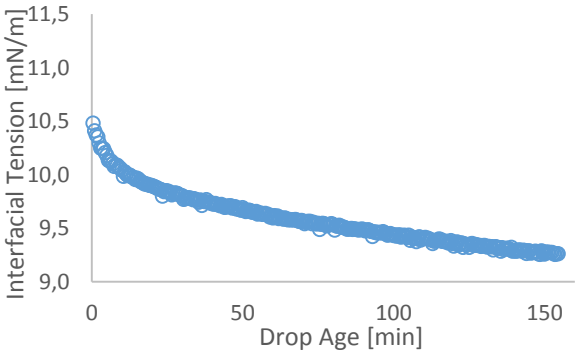

Figure A24. Crude oil B. Brine: 2.40 M, pH 3.

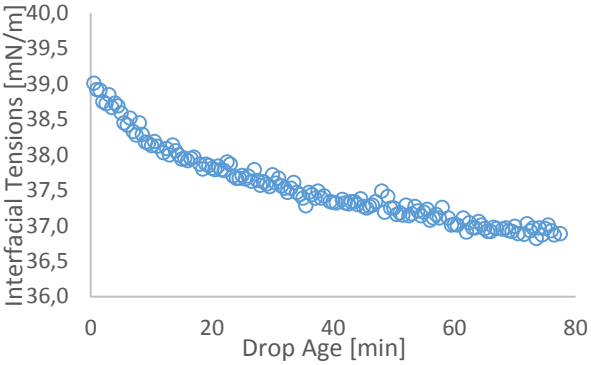

Figure A25. Crude oil B. Brine 0.03 M (Xca=0.04), pH 3.

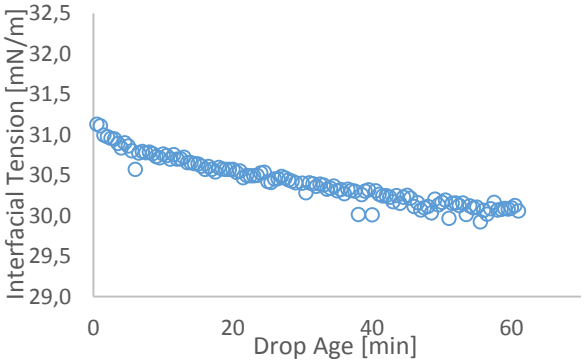

Figure A26. Crude oil B. Brine: 0.03 M, pH 6.

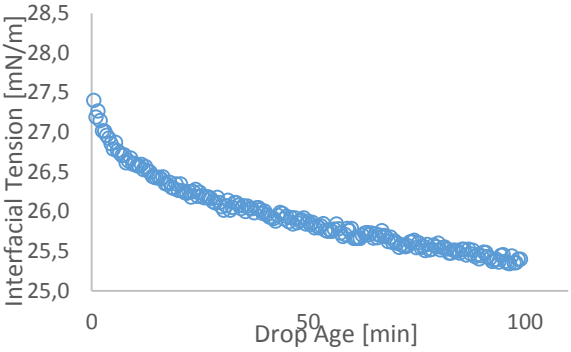

Figure A27. Crude oil B. Brine: 0.12 M, pH6.

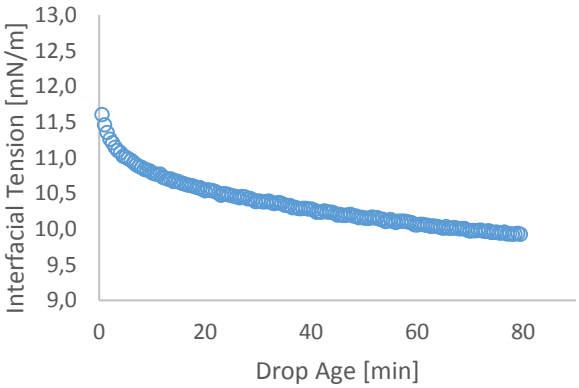

Figure A28. Crude oil B. Brine: 2.40 M, pH 6.

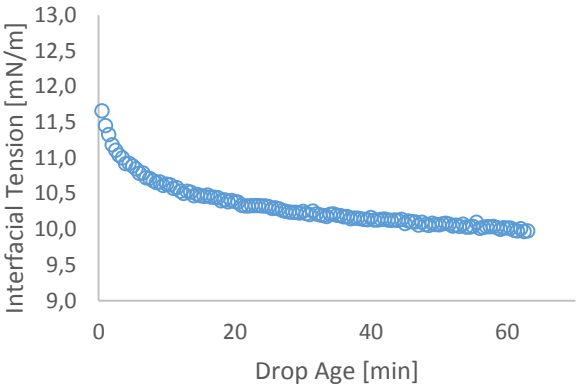

Figure A29. Crude oil B. Brine: 2.40 M, pH 6.

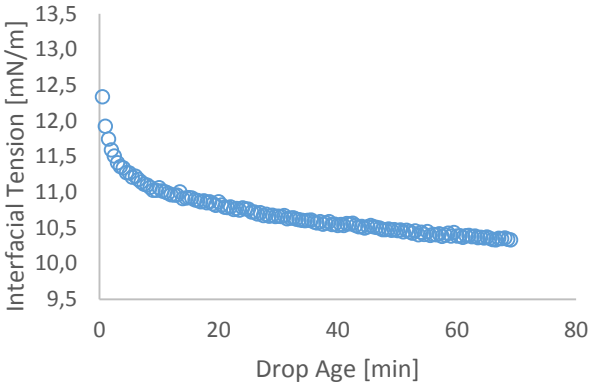

Figure A30. Crude oil B. Brine: 2.40 M, pH 6.

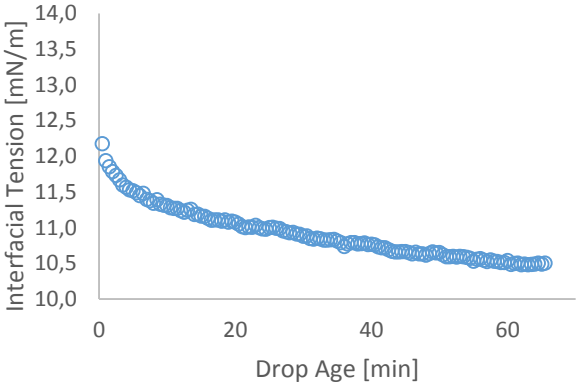

Figure A31. Crude oil B. Brine: 2.40 M, pH 6.

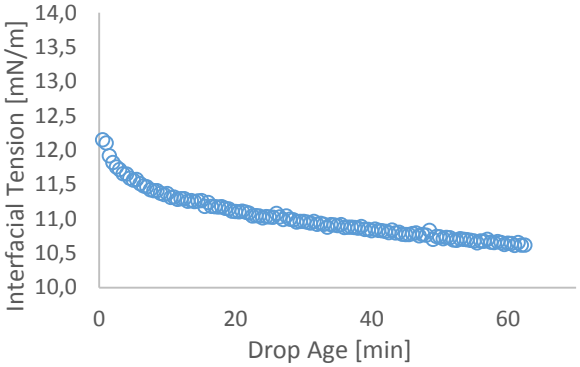

Figure A32. Crude oil B. Brine: 2.40 M, pH 6.

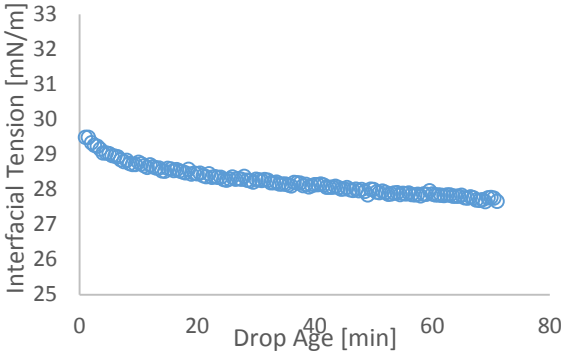

Figure A33. Crude oil B. Brine: 0.03 M (Xca=0.04), pH6.

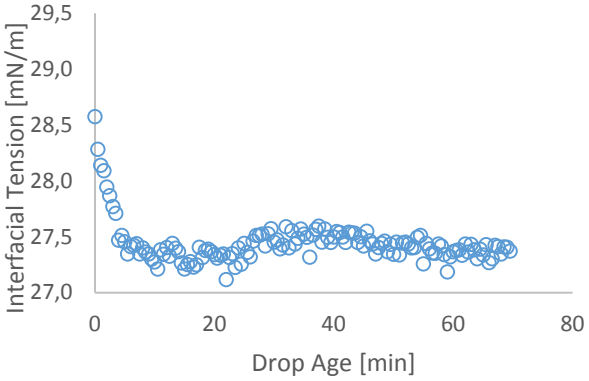

Figure A34. Crude oil B. Brine: 0.03 M, pH9.

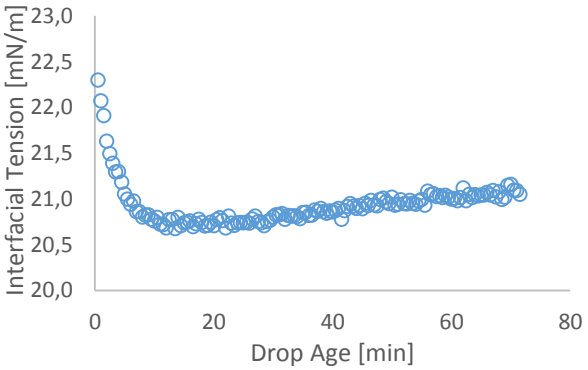

Figure A35. Crude oil B. Brine: 0.12 M, pH 9.

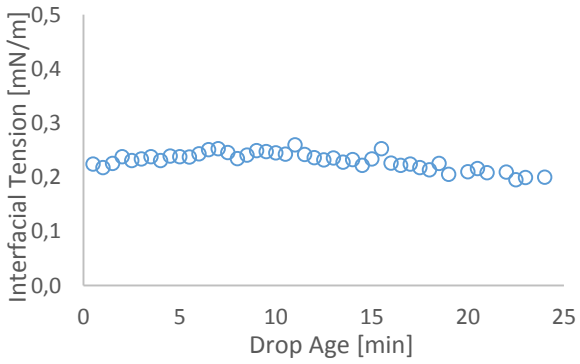

Figure A36. Crude oil B. Brine: 2.40 M, pH 9.

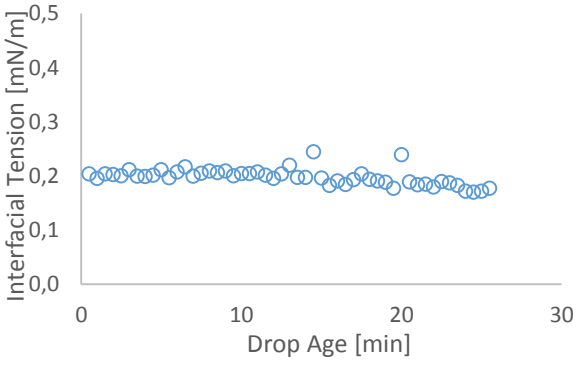

Figure A37. Crude oil B. Brine: 2.40 M, pH 9.

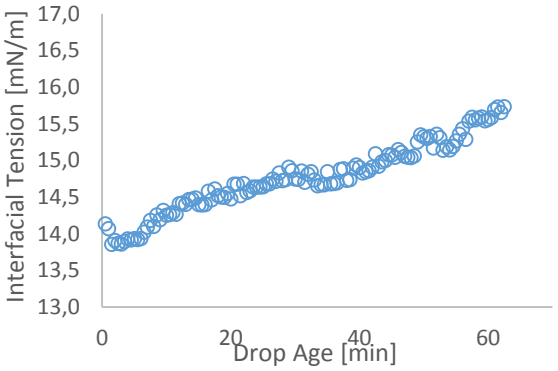

Figure A38. Crude oil B. Brine: 0.03 M (Xca=0.04), pH9.

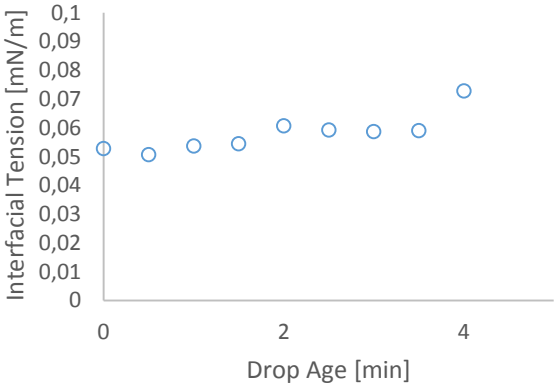

Figure A39. Crude oil B. Brine: 0.03 M, pH 11.

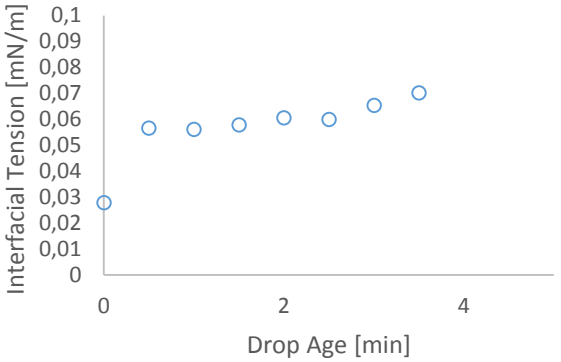

Figure A40. Crude oil B. Brine: 0.03 M, pH 11.

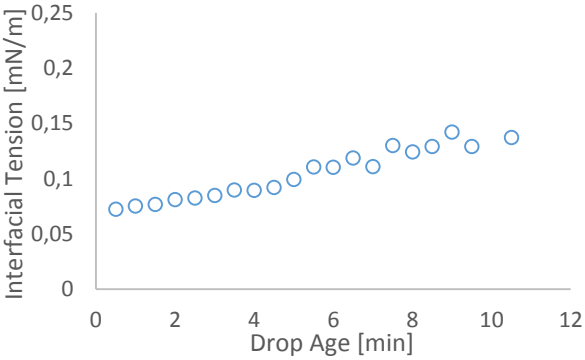

Figure A41. Crude oil B. Brine: 0.12 M, pH 11.

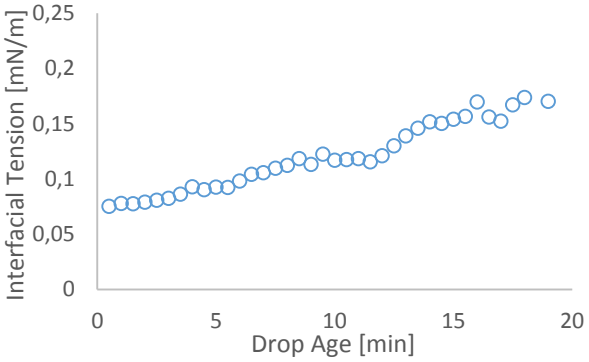

Figure A42. Crude oil B. Brine: 0.12 M, pH 11.

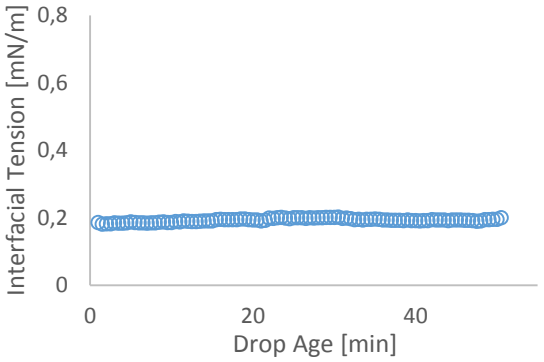

Figure A43. Crude oil B. Brine: 2.40 M, pH 11.

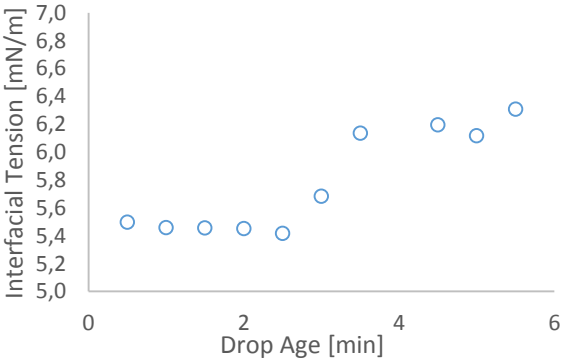

Figure A44. Crude oil B. Brine: 0.03 M (Xca=0.04), pH 11.

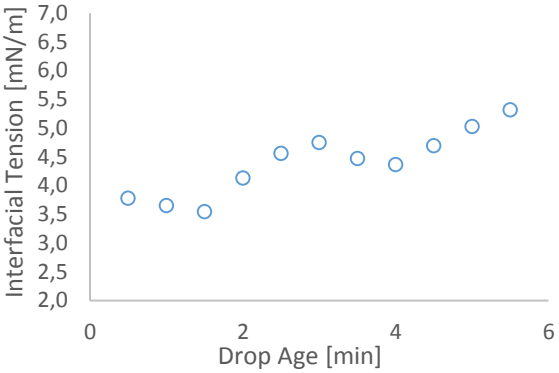

Figure A45. Crude oil B. Brine: 0.03 M (Xca=0.04), pH 11.

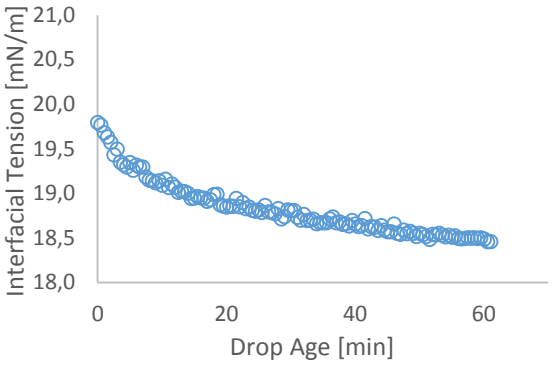

Figure A46. Crude oil C. Brine: 0.03 M, pH 3.

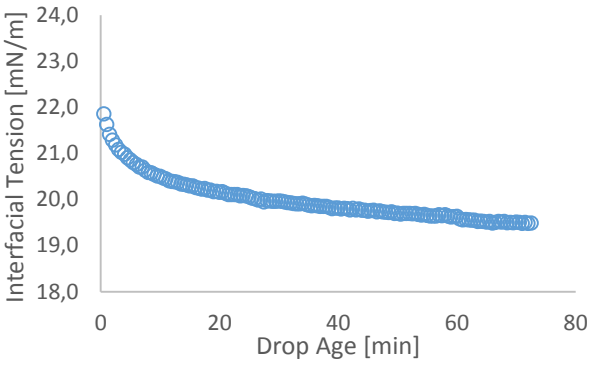

Figure A47. Crude oil C. Brine: 0.03 M, pH 3.

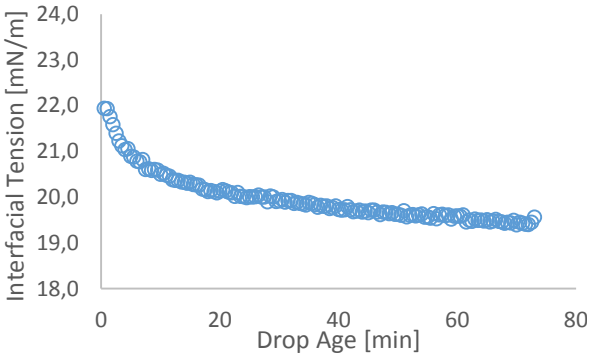

Figure A48. Crude oil C. Brine: 0.03 M, pH 3.

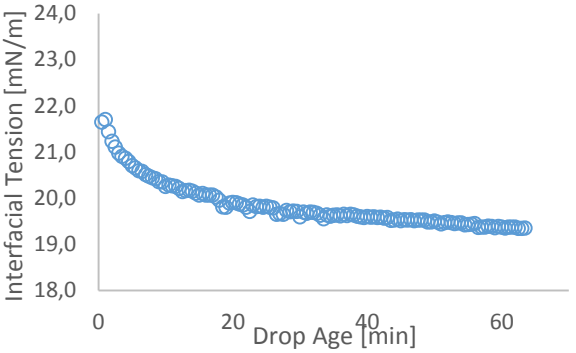

Figure A49. Crude oil C. Brine: 0.03 M, pH 3.

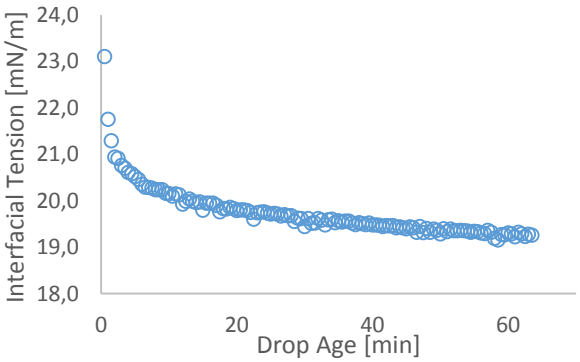

Figure A50. Crude oil C. Brine: 0.03 M, pH 3.

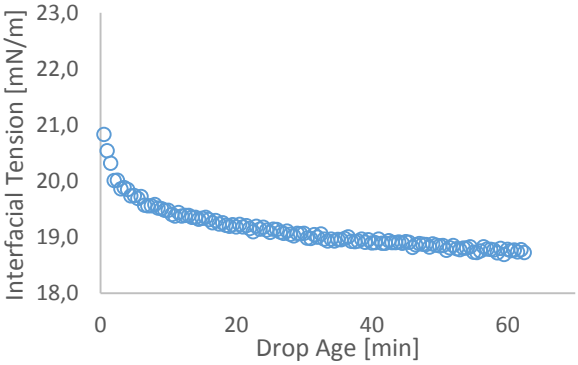

Figure A51. Crude oil C. Brine: 0.03 M, pH 3.

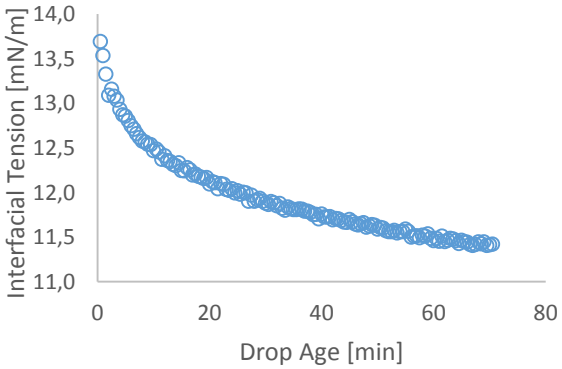

Figure A52. Crude oil C. Brine: 2.40 M, pH3.

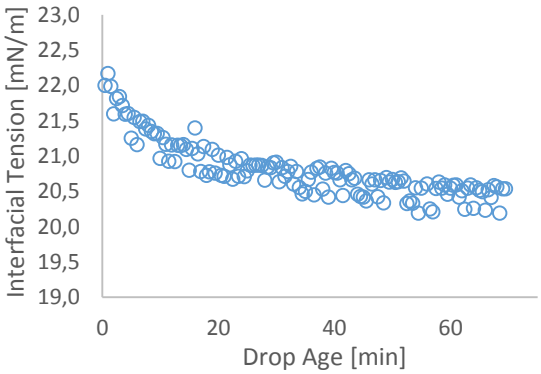

Figure A53. Crude oil C. Brine: 0.03 M (Xca=0.04), pH3.

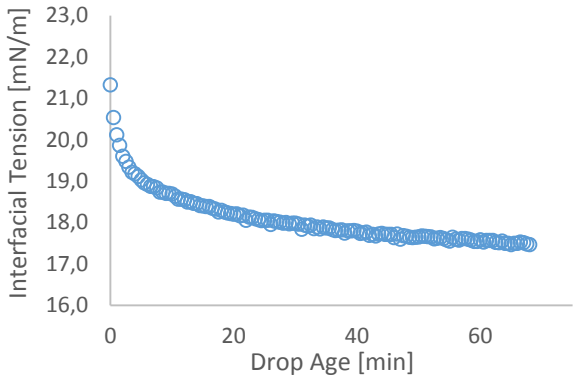

Figure A54. Crude oil C. Brine: 0.03 M, pH 6.

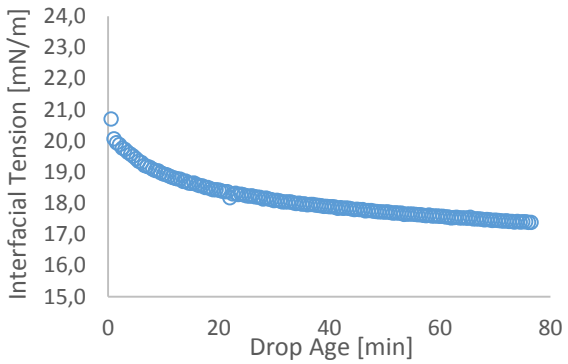

Figure A55. Crude oil C. Brine: 0.12 M, pH6.

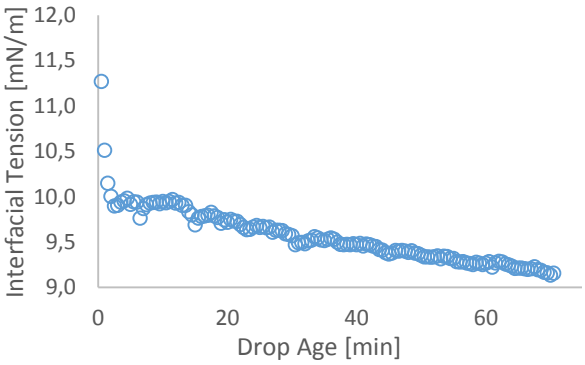

Figure A56. Crude oil C. Brine: 2.40 M, pH 6.

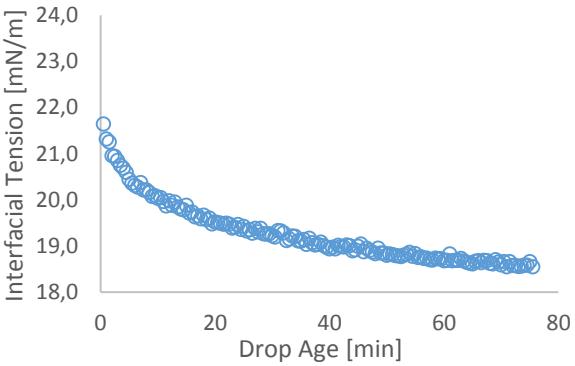

Figure A57. Crude oil C. Brine: 0.03 M (Xca=0.04), pH6.

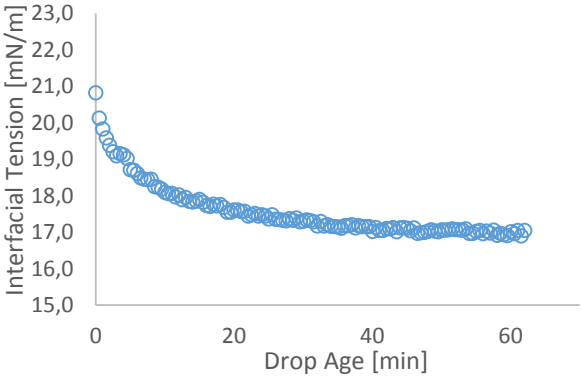

Figure A58. Crude oil C. Brine: 0.03 M, pH 9.

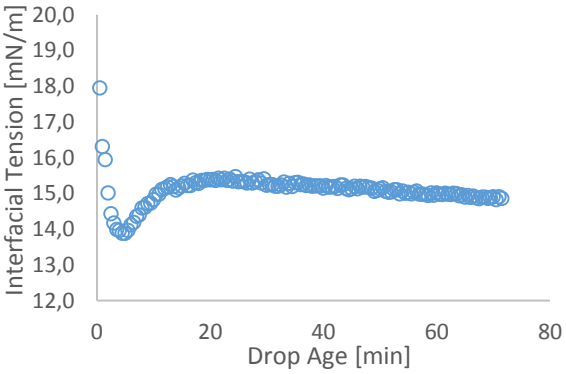

Figure A59. Crude oil C. Brine: 0.12 M, pH 9.

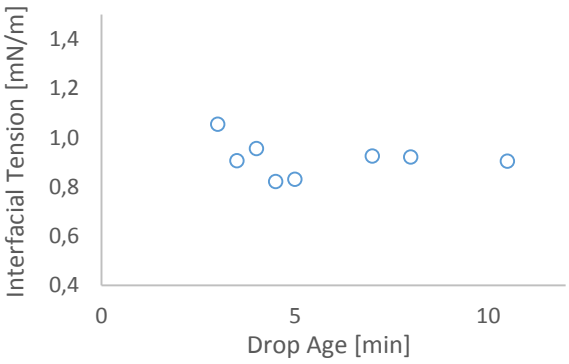

Figure A60. Crude oil C. Brine: 2.40 M, pH 9.

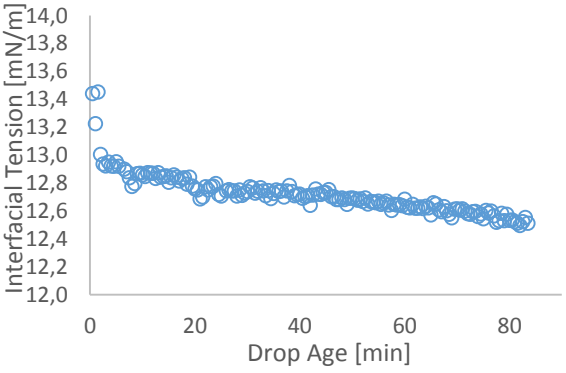

Figure A61. Crude oil C. Brine: 0.03 M (Xca=0.04), pH 9.

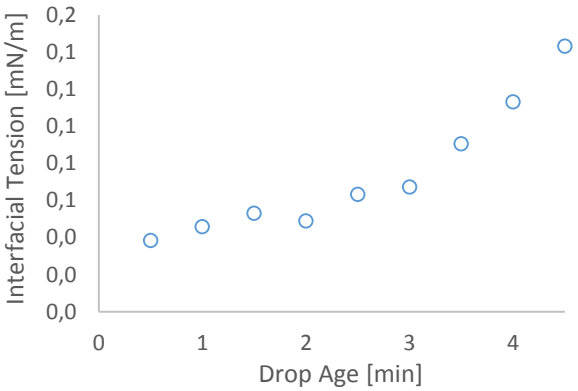

Figure A62. Crude oil C. Brine: 0.12 M, pH 9.

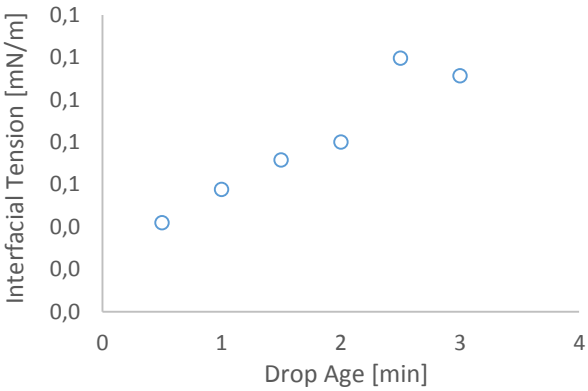

Figure A63. Crude oil C. Brine: 0.12 M, pH 9.

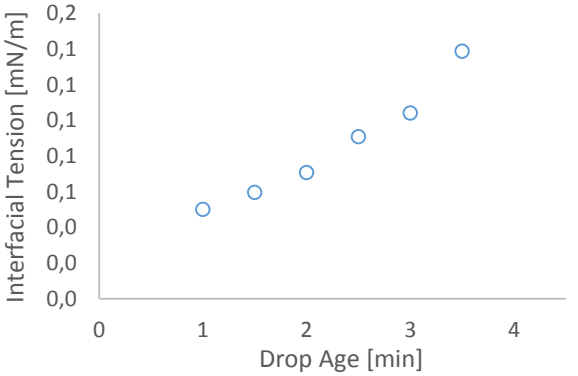

Figure A64. Crude oil C. Brine: 0.12 M, pH 9.

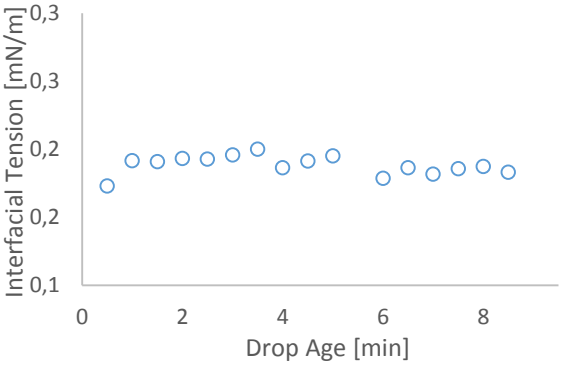

Figure A65. Crude oil C. Brine: 2.40 M, pH 11.

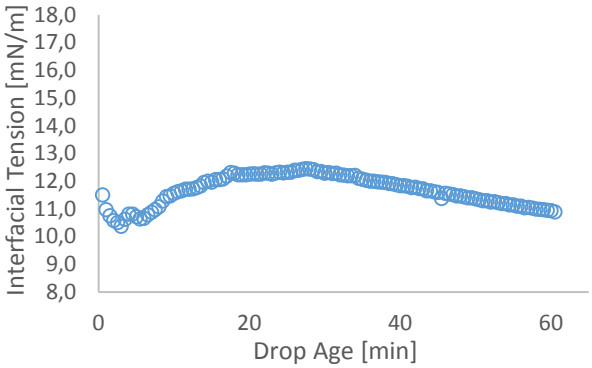

Figure A66. Crude oil C. Brine: 0.03 M (Xca=0.04), pH 11.

Appendix III: Zeta Potential Results

Table A-4. Measured zeta potential for crude oil A.

Brine (Ionic Strength [M])	Zeta Potential [mV]					
	pH 3	**pH 4**	**pH 6**	**pH 8**	**pH 9**	**pH 11**
0.006 M	43 ± 7	7 ± 4	-36 ± 3	-69 ± 6	-68 ± 6	-104 ± 9
	45 ± 5	7 ± 5	-36 ± 3	-76 ± 6	-64 ± 5	-105 ± 9
	45 ± 6	7 ± 4	-38 ± 4	-73 ± 6	-61 ± 5	-104 ± 9
	-	8 ± 6	-36 ± 3	-	-	-110 ± 11
	-	7 ± 5	-37 ± 4	-	-	-116 ± 9
	-	8 ± 4	-37 ± 4	-	-	-117 ± 10
	-	8 ± 3	-39 ± 4	-	-	-113 ± 10
	-	7 ± 5	-39 ± 5	-	-	-112 ± 10
	-	8 ± 4	-40 ± 5	-	-	-115 ± 10
	-	7 ± 3	-43 ± 5	-	-	-117 ± 9
Average	**44 ± 6**	**7 ± 4**	**-38 ± 5**	**-73 ± 7**	**-64 ± 6**	**-111 ± 11**
0.03 M	23 ± 7	8 ± 8	-25 ± 8	-66 ± 7	-72 ± 8	-92 ± 10
	29 ± 8	8 ± 10	-25 ± 8	-60 ± 7	-81 ± 13	-111 ± 8
	-	-	-24 ± 5	-	-	-103 ± 13
Average	**26 ± 8**	**8 ± 9**	**-30 ± 7**	**-63 ± 8**	**-76 ± 12**	**-102 ± 13**
0.03 M (X_{Ca}=0.04)	27 ± 8	-12 ± 9	-36 ± 9	-45 ± 4	-50 ± 11	-98 ± 22
	24 ± 11	-15 ± 6	-37 ± 9	-50 ± 4	-	-96 ± 18
	-	-	-	-	-	-96 ± 28
Average	**25 ± 10**	**-13 ± 8**	**-37 ± 10**	**-48 ± 16**	**-50 ± 11**	**-96 ± 23**
0.12 M	5	-8	-10	-29	-37	-55
	6	-10	-13	-36	-36	-61
	6	-8	-11	-30	-36	-59
	5	-9	-11	-	-	-62
	6	-10	-11	-	-	-64
	5	-14	-11	-	-	-64
	-	-	-12	-	-	-66
	-	-	-12	-	-	-66
	-	-	-14	-	-	-67
	-	-	-13	-	-	-68
Average	**6 ± 0**	**-10 ± 2**	**-12 ± 2**	**-32 ± 3**	**-37 ± 0**	**-64 ± 4**

Table A-5. Measured zeta potential for crude oil B.

Brine (Ionic Strength [M])	Zeta Potential [mV]					
	pH 3	**pH 4**	**pH 6**	**pH 8**	**pH 9**	**pH 11**
0.006 M	77 ± 6	37 ± 4	-25 ± 4	-84 ± 5	-51 ± 7	-104 ± 10
	79 ± 5	39 ± 4	-28 ± 4	-84 ± 6	-57 ± 6	-104 ± 10
	79 ± 5	36 ± 4	-27 ± 5	-86 ± 7	-59 ± 6	-108 ± 9
	82 ± 4	-	-27 ± 4	-88 ± 6	-	-108 ± 10
	79 ± 4	-	-28 ± 4	-89 ± 6	-	-102 ± 9
	81 ± 7	-	-30 ± 5	-	-	-103 ± 9
	-	-	-	-	-	-104 ± 8
	-	-	-	-	-	-104 ± 9
	-	-	-	-	-	-105 ± 9
	-	-	-	-	-	-107 ± 9
Average	**80 ± 5**	**37 ± 4**	**-27 ± 5**	**-86 ± 6**	**-57 ± 7**	**-105 ± 10**
0.03 M	47 ± 9	31 ± 7	-16 ± 7	-62 ± 11	-87 ± 7	-85 ± 10
	36 ± 7	33 ± 6	-	-59 ± 8	-87 ± 5	-94 ± 12
	-	-	-	-	-	-87 ± 10
Average	**41 ± 10**	**32 ± 7**	**-16 ± 7**	**-61 ± 9**	**-87 ± 13**	**-89 ± 11**
0.03 M (X_{Ca}=0.04)	35 ± 7	35 ± 8	-22 ± 8	-50 ± 9	-55 ± 9	-94 ± 17
	42 ± 7	34 ± 13	-27 ± 7	-46 ± 9	-62 ± 7	-99 ± 12
	47 ± 9	26 ± 8	-	-49 ± 11	-	-96 ± 20
	-	-	-	-53 ± 9	-	-
	-	-	-	-57 ± 9	-	-
Average	**41 ± 9**	**32 ± 10**	**-24 ± 7**	**-51 ± 10**	**-59 ± 9**	**-91 ± 21**
0.12 M	28	4	-13	-31	-22	-40
	30	5	-17	-27	-28	-39
	31	6	-15	-30	-22	-39
	28	-	-16	-	-	-36
	30	-	-17	-	-	-39
	-	-	-	-	-	-39
	-	-	-	-	-	-40
	-	-	-	-	-	-40
	-	-	-	-	-	-38
	-	-	-	-	-	-43
Average	**29 ± 1**	**5 ± 1**	**-16 ± 1**	**-29 ± 3**	**-22 ± 0**	**-39 ± 4**

Table A-6. Measured zeta potential for crude oil C.

Brine (Ionic Strength [M])	Zeta Potential [mV]					
	pH 3	**pH 4**	**pH 6**	**pH 8**	**pH 9**	**pH 11**
0.006 M	29 ± 5	-9 ± 4	-24 ± 6	-86 ± 7	-66 ± 7	-99 ± 8
	33 ± 4	-9 ± 4	-25 ± 6	-81 ± 6	-66 ± 7	-107 ± 8
	32 ± 5	-9 ± 4	-26 ± 5	-86 ± 8	-70 ± 8	-105 ± 9
	-	-10 ± 4	-	-82 ± 7	-	-
	-	-10 ± 4	-	-80 ± 7	-	-
	-	-10 ± 5	-	-82 ± 8	-	-
	-	-9 ± 5	-	-79 ± 7	-	-
	-	-9 ± 4	-	-	-	-
	-	-9 ± 4	-	-	-	-
	-	-10 ± 4	-	-	-	-
Average	**31 ± 5**	**-10 ± 4**	**-25 ± 6**	**-81 ± 7**	**-67 ± 8**	**-104 ± 9**
0.03 M	21 ± 13	-9 ± 12	-37 ± 11	-47 ± 8	-52 ± 7	-105 ± 14
	23 ± 11	-10 ± 8	-46 ± 9	-43 ± 8	-57 ± 8	-102 ± 7
	-	-9 ± 9	-45 ± 10	-50 ± 8	-	-97 ± 10
Average	**22 ± 12**	**-9 ± 10**	**-43 ± 11**	**-46 ± 8**	**-54 ± 8**	**-101 ± 11**
0.03 M (X_{Ca}=0.04)	25 ± 6	-1 ± 5	-27 ± 5	-54 ± 7	-38 ± 11	-79 ± 8
	25 ± 9	-3 ± 6	-29 ± 8	-62 ± 11	-38 ± 12	-85 ± 16
	-	-	-	-56 ± 17	-41 ± 13	-86 ± 19
Average	**25 ± 7**	**-2 ± 6**	**-28 ± 7**	**-57 ± 13**	**-39 ± 12**	**-83 ± 16**
0.12 M	11	-15	-14	-32	-60	-61
	11	-12	-15	-27	-63	-65
	10	-15	-16	-21	-67	-66
	-	-17	-13	-23	-	-
	-	-	-14	-20	-	-
	-	-	-12	-25	-	-
	-	-	-	-24	-	-
	-	-	-	-26	-	-
	-	-	-	-23	-	-
	-	-	-	-25	-	-
Average	**11 ± 1**	**-15 ± 2**	**-14 ± 1**	**-24 ± 2**	**-64 ± 3**	**-64 ± 2**

Appendix IV: Contact Angle Results

Table A-7. Measured contact angles for crude oil A.

Brine (Ionic Strength [M])	**Contact Angle [°]**		
	pH 3	**pH 6**	**pH 9**
0.12 M	29	26	49
	30	29	48
	30	26	-
	30	28	-
	-	28	-
Average	**30 ± 1**	**27 ± 1**	**49 ± 1**
2.40 M	58	30	99
	57	29	96
	57	30	100
	57	29	93
	52	-	-
Average	**56 ± 2**	**30 ± 1**	**97 ± 3**
0.03 M (X_{Ca}=0.04)	38	27	45
	32	27	38
	32	28	48
	-	28	43
	-	-	37
Average	**34 ± 3**	**28 ± 1**	**42 ± 4**

Table A-8. Measured contact angles for crude oil B.

Brine (Ionic Strength [M])	Contact Angle [°]		
	pH 3	**pH 6**	**pH 9**
0.12 M	43	28	68
	38	33	71
	42	36	
		36	
		25	
		29	
Average	**40 ± 2**	**31 ± 4**	**70 ± 2**
2.40 M	40	57	60
	48	59	59
	46	57	60
	42	51	65
	39	52	62
Average	**43 ± 3**	**55 ± 3**	**61 ± 2**
0.03 M (X_{Ca}=0.04)	39	19	40
	43	17	34
	43	20	39
	45		36
	49		
Average	**44 ± 3**	**19 ± 1**	**37 ± 2**

Table A-9. Measured contact angles for crude oil C.

Brine (Ionic Strength [M])	Contact Angle [°]		
	pH 3	**pH 6**	**pH 9**
0.12 M	51	32	63
	56	32	56
	59	37	60
		33	
		27	
Average	**22 ± 5**	**32 ± 3**	**60 ± 3**
2.40 M	63	56	54
	62	59	55
		59	58
		60	56
			59
			57
Average	**63 ± 1**	**59 ± 1**	**57 ± 2**
0.03 M (X_{Ca}=0.04)	55	50	52
	53	57	54
	52	47	58
		50	60
			49
Average	**54 ± 1**	**51 ± 4**	**55 ± 4**